Rates of rockwall slope erosion in the upper Bhagirathi catchment, Garhwal Himalaya

Elizabeth N. Orr,[1,2]* (iD) **Lewis A. Owen,**[1,3] **Sourav Saha**[1,4] (iD) **and Marc W. Caffee**[5,6]
[1] Department of Geology, University of Cincinnati, Cincinnati, OH 45221, USA
[2] GFZ German Research Centre for Geosciences, Telegrafenberg, 14473 Potsdam, Germany
[3] Department of Marine, Earth, and Atmospheric Sciences, North Carolina State University, Raleigh, NC 27695, USA
[4] Department of Earth, Planetary, and Space Sciences, University of California, Los Angeles, CA 90095, USA
[5] Department of Physics, Purdue University, West Lafayette, IN 47907, USA
[6] Department of Earth, Atmospheric and Planetary Sciences, Purdue University, West Lafayette, IN 47907, USA

*Correspondence to: Elizabeth N. Orr, Department of Geology, University of Cincinnati, Cincinnati, OH 45221, USA.
E-mail: elizabeth.orr@gfz-potsdam.de, orreh@mail.uc.edu

ESPL
Earth Surface Processes and Landforms

ABSTRACT: Rockwall slope erosion is defined for the upper Bhagirathi catchment using cosmogenic Beryllium-10 (^{10}Be) concentrations in sediment from medial moraines on Gangotri glacier. Beryllium-10 concentrations range from 1.1 ± 0.2 to $2.7 \pm 0.3 \times 10^4$ at/g SiO_2, yielding rockwall slope erosion rates from 2.4 ± 0.4 to 6.9 ± 1.9 mm/a. Slope erosion rates are likely to have varied over space and time and responded to shifts in climate, geomorphic and/or tectonic regime throughout the late Quaternary. Geomorphic and sedimentological analyses confirm that the moraines are predominantly composed of rockfall and avalanche debris mobilized from steep relief rockwall slopes via periglacial weathering processes. The glacial rockwall slope erosion affects sediment flux and storage of snow and ice at the catchment head on diurnal to millennial timescales, and more broadly influences catchment configuration and relief, glacier dynamics and microclimates. The slope erosion rates exceed the averaged catchment-wide and exhumation rates of Bhagirathi and the Garhwal region on geomorphic timescales ($10^3 - 10^5$ years), supporting the view that erosion at the headwaters can outpace the wider catchment. The ^{10}Be concentrations of medial moraine sediment for the upper Bhagirathi catchment and the catchments of Chhota Shigri in Lahul, northern India and Baltoro glacier in Central Karakoram, Pakistan show a tentative relationship between ^{10}Be concentration and precipitation. As such there is more rapid glacial rockwall slope erosion in the monsoon-influenced Lesser and Greater Himalaya compared to the semi-arid interior of the orogen. Rockwall slope erosion in the three study areas, and more broadly across the northwest Himalaya is likely governed by individual catchment dynamics that vary across space and time. © 2019 The Authors. Earth Surface Processes and Landforms Published by John Wiley & Sons, Ltd.

KEYWORDS: supraglacial processes; sediment flux; glacier; climate; cosmogenic isotopes

Introduction

Glaciation and glacial erosion are central to the topographic evolution of high-altitude mountain belts such as the Himalayan-Tibetan orogen, by influencing rates of sedimentation and localized incision, limiting relief production and elevation, and offsetting tectonic uplift (Brozović *et al.*, 1997; Whipple *et al.*, 1999; Mitchell and Montgomery, 2006; Wulf *et al.*, 2010, 2011; Scherler *et al.*, 2014). The contributions of periglacial erosion at the catchment head to the denudation budgets of Himalayan glacierized catchments have been largely overlooked, with the exception of studies by Heimsath and McGlynn (2008) in the Nepal High Himalaya and Seong *et al.* (2009) in the Central Karakoram of Pakistan. This is surprising given that lateral slope erosion via periglacial processes are shown to exceed

rates of glacial incision in other alpine settings (Brocklehurst and Whipple, 2006; Foster *et al.*, 2008).

Periglacial weathering processes including freeze–thaw, frost cracking and ice wedging deliver large volumes of rockfall and avalanche debris to the mountain glacier sedimentary system from catchment slopes (Schroder *et al.*, 2000; Matsuoka, 2001; Owen *et al.*, 2003; Hales and Roering, 2005; Sanders *et al.*, 2012; Gibson *et al.*, 2017). The strength of coupling between rockwall slopes and glaciers affect glacier dynamics, catchment sediment flux and can dictate the relief and topographic configuration of catchment divides over time (Montgomery, 2002; Thiede *et al.*, 2005; Moore *et al.*, 2009). Erosion of rockwall slopes in the Himalayan-Tibetan orogen therefore has broad implications for its morphological development and the distribution of precipitation (Burbank *et al.*, 2003; Gabet *et al.*, 2004; Anders *et al.*, 2006; Bookhagen and Burbank, 2006).

The distribution and rates of erosion for the Himalayan-Tibetan orogen scale with tectonics (Burbank *et al.*, 2003;

The copyright line for this article was changed on 12 March 2020 after original online publication.

Thiede *et al.*, 2005; Scherler *et al.*, 2014) precipitation (Thiede *et al.*, 2004; Grujic *et al.*, 2006; Biswas *et al.*, 2007; Craddock *et al.*, 2007; Gabet *et al.*, 2008; Wulf *et al.*, 2010; Deeken *et al.*, 2011; Portenga *et al.*, 2015) and/or topography (Vance *et al.*, 2003; Scherler *et al.*, 2011a, 2014). Erosion at the catchment head is shown to outpace catchment-wide and regional landscape denudation rates, and exhibit greater or different sensitivities to local and/or regional external forcing such as shifts in climate, tectonic activity or geomorphic regime (Heimsath and McGlynn, 2008; Scherler *et al.*, 2011a). We aim to assess the importance of periglacial processes in the Himalayan-Tibetan orogen; an essential first step is the quantification of rockwall slope erosion rates. We chose the upper Bhagirathi catchment of the Garhwal Himalaya, northern India, for this initial investigation. This region is the source area for the Ganges and it contains some of the largest glaciers in the monsoon-influenced Himalaya, including Gangotri glacier. This catchment has a well-defined glacial chronostratigraphy, comprehensive records of past and modern glacier behavior and is relatively accessible. We apply geomorphic and sedimentological methods and measure cosmogenic beryllium-10 (^{10}Be) concentrations in medial moraine sediment to calculate rockwall slope erosion rates. Moreover by comparing ^{10}Be concentrations along the length of the medial moraines and examining the sedimentology of the supraglacial sediment, we are able assess the feasibility of using ^{10}Be to determine rates of rockwall slope erosion. We compare our erosion rates to local catchment-wide erosion and exhumation records to assess the difference between rockwall slope erosion and regional landscape denudation in Garhwal. We compare slope erosion rates for upper Bhagirathi, Chhota Shigri in the Lahul Himalaya, northern India and Baltoro in the Central Karakoram of Pakistan with catchment parameters and regional climate

records to help identify the factors that may be affecting slope erosion in the northwest (NW) Himalaya.

Regional Setting

The Bhagirathi catchment is located in the Uttarkashi district of Uttarakhand, in the Garhwal Himalaya of northern India (Figure 1). Three major lithotectonic units characterize the geology of the Garhwal Himalaya: (1) Tethyan Himalaya sedimentary series; (2) the high Himalaya crystalline sequence (HHS); and (3) the lesser Himalaya sequence (LHS; Searle *et al.*, 1997, 1999; Vannay *et al.*, 2004). Despite the absence of a clear shear zone, Garhwal is bounded in the north by the Tethyan Himalaya low-grade metasedimentary rocks and the south Tibetan detachment (STD) zone (Kumar *et al.*, 2009; Srivastava, 2012). The main central thrust zone defines the southern margin of the region; the boundary between high-grade gneiss, migmatite and granite of the HHS and low-grade metasedimentary rocks of the LHS. The Jhala normal fault trends through central Garhwal and the Bhagirathi catchment, separating quartzo-feldpathic sillimanite gneiss from Harsil metasedimentary rocks (Searle *et al.*, 1999). Maximum regional uplift rates range between 4 and 5.7 mm/a (Barnard *et al.*, 2004a, 2004b; Scherler *et al.*, 2014). Neotectonics, which include persistent microseismicity and stochastic earthquakes, greatly influence the geomorphic evolution of the region (Searle *et al.*, 1987; Valdiya, 1991; Rajendran *et al.*, 2000; Barnard *et al.*, 2001; Bali *et al.*, 2003). Detailed summaries of the geologic setting and histories of transient erosion, unroofing and exhumation for Garhwal are provided by Scaillet *et al.* (1995), Searle *et al.* (1993, 1999), Sorkhabi *et al.* (1996) and Scherler *et al.* (2014).
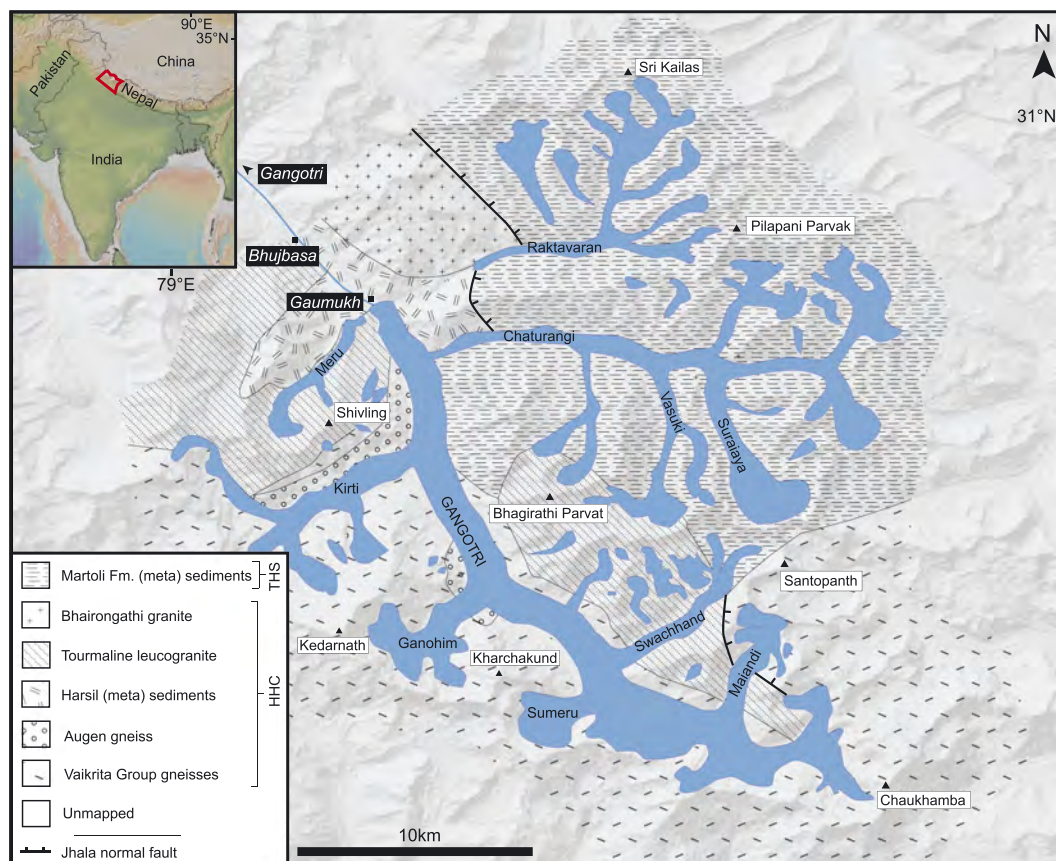

Figure 1. Location of Gangotri glacier and tributary glaciers overlying a simplified geologic map of the upper Bhagirathi basin of Uttarkashi, northern India (adapted from Searle *et al.*, 1999). Inset map illustrates the location of the state of Uttarakhand within the Himalayan-Tibetan orogen (base map from geomapapp.org). [Colour figure can be viewed at wileyonlinelibrary.com]

The climate of the western Himalaya is influenced by two major climatic systems, the southwest Indian monsoon and the northern hemispheric mid-latitude westerlies (Finkel *et al.*, 2003; Bookhagen *et al.*, 2005; Owen, 2009). The majority of annual precipitation (1000−2500 mm/a) in Garhwal occurs between July and September; during this time the humid air masses of the Indian monsoon penetrate the high-altitude ranges of the Greater Himalaya (Burbank *et al.*, 2003; Scherler *et al.*, 2010; Thayyen and Gergan, 2010; Wulf *et al.*, 2010). Rainfall magnitudes vary significantly both seasonally and across short distances (10^1 to 10^2 km) throughout the region, creating localized microclimates that are affected by the variability in terrain and geomorphic regime (Sharma and Owen, 1996; Barros *et al.*, 2006; Singh *et al.*, 2007; Srivastava, 2012).

Due to the restricted number of meteorological stations located above ~5000 m above sea level (a.s.l.) in the Himalaya (Benn *et al.*, 2012; Srivastava, 2012), climate and weather records for the upper Bhagirathi catchment are traditionally based on data from a single weather station (Mukhim, 30.6°N, 78.3°E, ~1900 m a.s.l.). Mukhim station (1971−2000) records mean annual precipitation of 1648 mm and temperature of 15.5°C. An additional weather station has been established at Bhojbasa (~3780 m a.s.l., 30.9°N, 79.0°E), ~4 km from the snout of Gangotri glacier. Temperatures range between -2.3 and 11°C (2001–2009) each year. The station has documented a mean annual winter snowfall of ~546 mm (Bhambri *et al.*, 2011).

The upper Bhagirathi catchment (3400–7200 m a.s.l.) covers an area of ~550 km^2, of which ~50% is glaciated (Tangri *et al.*, 2004; Haritashya *et al.*, 2006; Singh *et al.*, 2006). This transverse catchment is delineated by steep relief peaks (> 45° [averaged over ~770 km^2]) that exceed 6000 m a.s.l., including Shivling (6543 m a.s.l.), Meru (6660 m a.s.l.) and the Chaukhamba Massif (7138 m a.s.l.; Bhambri *et al.*, 2011; Satyabala, 2016). Alpine shrubs and grasses with some sandy-gravel soil development are sparsely distributed or absent above elevations of ~3000 m a.s.l. Below Gaumukh (~4000 m a.s.l., 30.9 °N, 79.1°E), the catchment is unglaciated and becomes wider and deeper as a result of the calving of a steep gorge by the Bhagirathi River. Alpine tundra vegetation transforms to montane forests between ~3000 and 1000 m a.s.l. (Schweinfurth, 1968; Srivastava, 2012). River terraces are present along the valley floors, most of which are cultivated.

The upper Bhagirathi catchment preserves an abundance of moraines, debris flow/alluvial fans and cones, strath/fill terraces and landslides (Owen and Sharma, 1998; Burbank *et al.*, 2003; Singh *et al.*, 2017). Mass movements are particularly prevalent throughout the region as a consequence of glacial and fluvial erosion, heavy monsoon rains, localized storms and earthquakes, which each enhance slope instability (Owen *et al.*, 1996; Barnard *et al.*, 2001, 2004a, 2004b).

Gangotri glacier is the largest glacier (~30-km-long) in the drainage basin. This temperate glacier is fed by a series of 10 smaller tributary glaciers including Chaturangi and Kirti between elevations of ~4005 and 5950 m a.s.l. (Dutta *et al.*, 2004; Srivastava, 2012, Haritashya *et al.*, 2006). Gangotri glacier has an estimated volume of ~20 to 30 km^3 (Frey *et al.*, 2012; Bhattacharya *et al.*, 2016), a thickness ranging from 350 to 450 m in the accumulation zone and 40 to 65 m at its snout (Srivastava, 2012; Gantayat *et al.*, 2014; Singh *et al.*, 2017). The mean glacier surface velocity of Gangotri is ~48 ± 4.8 m/a (Bhattacharya *et al.*, 2016), and the contemporary equilibrium-line altitude (ELA) is between ~4510 and 5160 m a.s.l. (Owen and Sharma, 1998; Naithani *et al.*, 2001; Ahmad *et al.*, 2004, Burbank *et al.*, 2003; Srivastava, 2012; Singh *et al.*, 2017). Medial moraines of variable thickness (≤ 10 m) are present below the ELA, partially mantling the ~26-km-long ablation zone (Haritashya *et al.*, 2010; Scherler *et al.*, 2011a; Satyabala,

2016; Srivastava, 2012). Gangotri glacier has an undulating surface characterized by steep relief ridges and depressions, meltwater channels, drainage ponds and ice collapse features. Large lateral moraines trend parallel to the glacier along the lower ~10 km of the ablation zone, helping to form a series of discontinuous ablation valleys that are in-filled by hillslope and avalanche debris. Lacustrine deposits are present at Tapovan (4330 m a.s.l., 30.9°N, 79.1°E; Sharma and Owen, 1996; Haritashya *et al.*, 2006; Ranhotra and Bhattacharya, 2013).

Seven glacial stages have been defined within the upper Bhagirathi catchment and include the: Bhagirathi (60–23 ka), Sudarshan (21–16 ka), Shivling (~5.2 ka), Gangotri (~2.4–1.9 ka), Bhujbasa (~1.7–0.5 ka), Meru (~0.3±0.1 ka) and Gaumukh (~0.3–0.2 ka; Sharma and Owen, 1996; Barnard *et al.*, 2004a, 2004b; Puri *et al.*, 2004; Srivastava, 2012; Singh *et al.*, 2017). The low erosion rates measured within the drainage basin (< 1 mm/a; Vance *et al.*, 2003) and wider region (0.15–5.4 mm/a; Haritashya *et al.*, 2006; Scherler *et al.*, 2014) aid in the preservation of glacial landforms across several glacial cycles. The moraine of the Bhagirathi stage (60–23 ka) is located ~30 km downstream from the present glacier snout and records the oldest and most extensive glaciation of the drainage basin. Gangotri glacier has retreated between 6 and 27 m/a over the past 50 years, but since 2007 has ceased retreat. Tangri (2002), Tangri *et al.* (2004), Bhambri *et al.* (2012), Srivastava (2012) and Bhattacharya *et al.* (2016) provide detailed summaries of the glacier stages and retreat.

Methodology

Background

Past studies have quantified rockwall slope erosion by dating and estimating the volume of slope deposits such as talus (Andre, 1997; Curry and Morris, 2004; Hinchliffe and Ballantyne, 2009; Siewert *et al.*, 2012), or modeling supraglacial debris flux (Heimsath and McGlynn, 2008; Gibson *et al.*, 2017). More recently, rockwall slope erosion has been measured using cosmogenic ^{10}Be in medial moraine sediment (Heimsath and McGlynn, 2008; Seong *et al.*, 2009; Ward and Anderson, 2011; Scherler and Egholm, 2017). The terrestrial cosmogenic nuclide (TCN) concentration of a substrate scales with clast size; concentrations are higher in boulders compared to coarse-fine sediment (Placzek *et al.*, 2014). TCN-derived-erosion rates from amalgamated sediment are considered to best reflect the average rate of erosion for an applicable area, and are treated as maximum estimates. Medial moraines form when rockfall and avalanche debris mobilized from the catchment slopes is exhumed to the ablation zone surface after being buried and transported englacially through the accumulation zone (Matsuoka and Sakai, 1999; Goodsell *et al.*, 2005; MacGregor *et al.*, 2009; Mitchell and Montgomery, 2006; Dunning *et al.*, 2015). The ^{10}Be concentrations in medial moraine sediment reflect the mean surface concentrations of the source area (Ward and Anderson, 2011). For a given medial moraine sediment package, the shorter the duration of exposure of the source rockwall slopes to cosmic rays, the lower the accumulation of ^{10}Be, and the faster the inferred slope erosion rate. On sub-millennial timescales the ^{10}Be concentrations are likely to reflect slope erosion via periglacial weathering processes, whereas over geomorphic timescales ($10^3 - 10^5$ years) the input is more likely affected by local or regional erosion rates (Gibson *et al.*, 2017). We combine TCN methods with geomorphic and sedimentological analyses of Gangotri glacier

medial moraines to constrain rates of rockwall slope erosion for the upper Bhagirathi catchment.

Field methods

A detailed geomorphic map of the upper Bhagirathi catchment was constructed in the field and then refined using Advanced Spaceborne Thermal Emission and Reflection Radiometer (ASTER) global digital elevation models (GDEMs; 30-m-resolution), Landsat Enhanced Thematic Mapper Plus (ETM+; 15-m-resolution) imagery, Google Earth Imagery and published topographic and geologic maps. Geomorphic and sedimentological techniques described by Benn and Owen (2002) were applied to identify and differentiate between landforms and sediment deposits.

Six major medial moraines were identified on the surface of Gangotri glacier system. Each landform originates from an area of glacier convergence and extends to a confluence with, and/or snout of Gangotri glacier (Figure 2). The debris of each medial moraine is sourced from the rockwalls that encompass the glacier(s) above this area of convergence. Ward and Anderson (2011) argue that the trajectory of the englacial transport of rockwall debris is deeper than for debris that has been transferred onto the glacier surface at lower elevations in the catchment. The rockwall debris is entombed within the glacier ice during this transport and therefore does not mix with other sources.

The name of each moraine includes the initial term SD (for supraglacial debris moraine) and a subscript letter from A–F. The moraine sourced from the Kirti tributary catchment is referred to as SD_A, for example. The $SD_{A–C}$ moraines are the focus of this study as they are the largest and most accessible moraines on the glacier, and extend throughout the ablation zones of Gangotri and Kirti glaciers, making them most likely to reflect rockwall slope erosion rates of the upper Bhagirathi catchment. The traditional moraine nomenclature, e.g. $M_{1–x}$, was not used to avoid confusion with Gangotri terminal and lateral moraines.

Sediment samples from each moraine were collected where possible at intervals from the snout of Gangotri to ~3 km up-glacier. The moraines were inaccessible beyond this point due to major instabilities in both hillslopes and the glacier surface. The samples were taken from high relief, stable and well-defined moraine ridges, to avoid input from external sources of sediment, including lateral moraines and hillslope deposits (Supporting Information Item 1). To ensure the sampling of ≥ 10 rockwall events per sample, the sampling locations were ≥ 200 m^2 in area and sediment was collected systematically along the moraine crests every 5−10 paces. Approximately 3 kg of amalgamated sediment was collected for each sample, with a grain size range of < 3 cm (clay-coarse gravels) applying bulk sediment sampling methods of Gale and Hoare (1991). Detailed sedimentological and geomorphic descriptions of the moraine were made at each sampling location.

Two samples were collected from the SD_A moraine, three from SD_B and one from SD_C. The samples were numbered in ascending order for each moraine, from the furthest up-glacier to the closest to the snout of Gangotri glacier. The G_{sup1} sample (subscript sup1), e.g., was collected at 4315 m a.s.l., ~3 km from the snout. The location of each sample was recorded using a handheld Garmin Etrex 30 global positioning system (GPS) unit and then photographed.
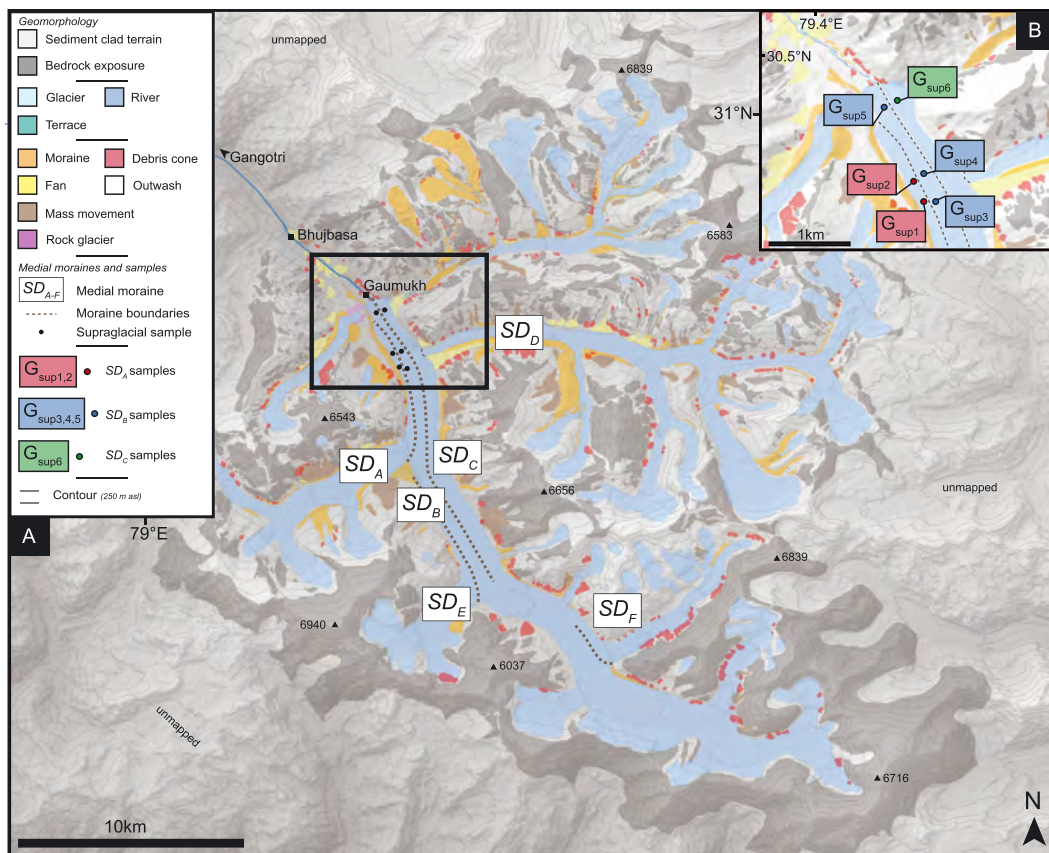

Figure 2. (A) Geomorphic map of the upper Bhagirathi catchment outlining the location of the five major supraglacial units ($SD_{A–F}$) of the Gangotri glacier system. Altitudinal zones of geomorphic landforms; moraine (~3900−6030 m a.s.l.), debris fan (~3890−5320 m a.s.l.), mass movement (4410−6020 m a.s.l.), rock glacier (~4440 m a.s.l.), debris cone (~3940−5900 m a.s.l.) and terrace (3890−4880 m a.s.l.). (B) Sample locations for each of the three investigated supraglacial units of this study. [Colour figure can be viewed at wileyonlinelibrary.com]

Medial moraine sediment analysis

To elucidate the characteristics and transport histories of the medial moraine sediment and to assist with interpreting the [10]Be inventories of our samples, analyses were conducted at the University of Cincinnati (OH, USA) in the Sedimentology and X-ray Laboratories in the Department of Geology and the Advanced Material Characterization Centre (AMCC). These analyses included grain size distribution (e.g. Wentworth, 1922; Allen, 1981), shape (e.g. Hambrey and Glasser, 2003; Hambrey *et al.*, 2008; Lukas *et al.*, 2013), roundness (e.g. Sneed and Folk, 1958; Ballantyne and Benn, 1994), surface weathering (e.g. Sheridan and Marshall, 1987; Owen *et al.*, 2003) and sample clay mineralogy (e.g. Chen, 1977; Moore and Reynolds, 1997). Further details of the methodologies used are provided in Supporting Information Item 2.

Beryllium-10 production rates and geochemical analysis

Beryllium-10 production rates for the upper Bhagirathi catchment were calculated from an ASTER GDEM (30-m-resolution) with a revised sea-level high-latitude spallogenic production rate of 4.08 ± 0.23 Be atoms/g SiO_2/a (Martin *et al.*, 2017; http://calibration.ice-d.org/) and [10]Be half-life of 1.36 Ma (Nishiizumi *et al.*, 2007), using methods of Dortch *et al.* (2011) in MATLAB R2017.a. The production rate for each pixel was corrected for topographic shielding and then averaged to derive the mean [10]Be production rate for the catchment. The mean production rates account for [10]Be production on the glacier surface.

Following the initial sedimentological analyses, the sediment fractions of each sample were combined, crushed, and re-sieved; the 250–500 μm fraction was selected for [10]Be analysis. This process minimizes the possibility of bias in the contribution of any one grain size to the geochemical analysis of the sample. Quartz isolation, dissolution, chromatography, isolation of Be and the preparation of beryllium oxide (BeO) were undertaken in the Geochronology Laboratories at the University of Cincinnati using the standards and chemical procedures described by Kohl and Nishiizumi (1992), Nishiizumi *et al.* (1994), and Dortch *et al.* (2009). The [10]Be/[9]Be of each sample were measured using accelerator mass spectrometry (AMS) at the Purdue Rare Isotope Measurement (PRIME) Laboratory at Purdue University, West Lafayette, IN, USA (Sharma *et al.*, 2000).

Portenga *et al.* (2015) have demonstrated that when native [9]Be is factored into [10]Be/[9]Be ratios, irrespective of geologic setting, the resultant [10]Be concentrations and inferred erosion rates can be significantly altered (20−400%). The native [9]Be measured in ~5 g fractions of clean quartz for each sample are < 1 ppm, so no adjustment to the [10]Be/[9]Be ratios was necessary. A procedural blank [10]Be/[9]Be ratio correction of $3 \pm 1 \times 10^{-15}$ was made for each sample. Muongenic production is negligible for the timescales of the processes characterized for this study (Brown *et al.*, 1995; Braucher *et al.*, 2003).

The accumulation of [10]Be between the rockwall and medial moraines (during burial, englacial transport and exhumation of sediment to the glacier surface) was calculated using the Ward and Anderson (2011) analytical model and then subtracted from the total [10]Be concentrations. Beryllium-10 accumulation during transport along the length of the medial moraine was found to be negligible. This conclusion is discussed further in the Results and Discussion sections. Rockwall slope erosion rates were calculated using the [10]Be concentrations and catchment-wide production rates by applying methods described in detail by Lal (1991), Granger *et al.* (1996), Balco *et al.* (2008) and Dortch *et al.* (2011).

Medial moraines in the Himalayan-Tibetan orogen including Bhagirathi are primarily composed of rockfall debris; smaller rockfall events occurring frequently across time and space, interjected by larger and less frequent events (Dunning *et al.*, 2007; Rowan *et al.*, 2015). Despite much of the volumetric erosion being achieved by these larger events, this bias within the sediment source in favor of small rockfall events means that the resultant erosion rates should be considered maximum estimates. Unique sediment exchange processes in the supraglacial environment (Ward and Anderson, 2011; Lukas *et al.*, 2012, 2013; Lupker *et al.*, 2012; Scherler *et al.*, 2015), shifts in sediment source, sediment storage and remobilization, shifting geomorphic regimes and ice/snow shielding (Bierman and Steig, 1996; Scherler *et al.*, 2014; Fame *et al.*, 2018) are also likely to affect the [10]Be concentrations and sediment characteristics of each sample. Caution must therefore be exercised when analyzing these data.

Interpreting the [10]Be concentrations of sediment in medial moraines is made more challenging because of the variability in production rates for alpine catchments and lack of uniformity in the [10]Be inventories at the bedrock surface, which vary over temporal and spatial scales. A detailed summary of this methodology and its assumptions are provided by Ward and Anderson (2011).

Topographic and geomorphic analyses

ASTER DEMs and Landsat ETM+ data were used in conjunction with geographic information system (GIS) Spatial Analyst tools for additional topographic analyses including catchment and rockwall slope, 3-km-radius relief, hypsometry and aspect. These parameters are defined for the glacial-periglacial realms of the upper Bhagirathi catchment only, as this is the area that pertains to the focus of our study. Topographic analyses of Chhota Shigri catchment in Lahul, northern India and Baltoro catchment in the Central Karakoram, Pakistan was also conducted to enable comparisons between slope erosion and catchment characteristics throughout the NW Himalaya.

An adiabatic environmental lapse rate $(\Delta T/\Delta Z)$ of 7°C/km, a product of both an approximate median for the orogen (Derbyshire *et al.*, 1991; De Scally, 1997; Thayyen *et al.*, 2005; Siddiqui and Maruthi, 2007; Bashir and Rasul, 2010; Pratap *et al.*, 2013; Kattel *et al.*, 2013, 2015), and a lapse rate derived from the local weather stations of Mukhim (~1900 m a.s.l.) and Bhojbasa (~3780 m a.s.l.; Bhambri *et al.*, 2011) was used to estimate the summer and winter surface temperatures throughout the upper Bhagirathi catchment. The optimum frost cracking envelope defined by Hales and Roering (2005) falls between mean annual temperatures of -8 and -3°C. Bhagirathi catchment elevations that have surface temperatures within this range were determined using the chosen lapse rate and ASTER DEM. The frost-cracking envelope and distribution of permafrost (0°C; Brown, 1970) was also calculated with respect to depth by modeling the thermal structure of the near surface of the catchment using methods outlined in detail by Anderson and Anderson (2010). A thermal diffusivity of 1.15 mm^2/s was used as it reflects an approximate midpoint in diffusivity values for the following substrates that characterize the catchment; regolith, landforms and deposits, and bedrock. This provides an estimate for the rate of heat transfer from the surface. Despite offering a reasonable assessment of the frost cracking and permafrost distribution, these simplified methodologies involve a series of assumptions about the physics, temperature data and geologic setting (Anderson and Anderson,

2010). Surface temperatures of upper Bhagirathi will have varied over space and time, a condition that must be accounted for when interpreting this data. These analyses aim to determine whether slope failure in the upper Bhagirathi catchment can be influenced by surface temperature and the associated periglacial weathering processes.

ELA and snowline altitude (SA) reconstructions

ELAs and ELA depressions (ΔELA) were calculated for the contemporary and past glacial stages within the upper Bhagirathi catchment using methods described by Osmaston (2005), Benn *et al.* (2005), Heyman (2014) and Sharma *et al.* (2000). To reduce the uncertainties inherent within these reconstructions, a mean ELA was calculated for each glacial stage from reconstructions derived from each of the following methods: area-altitude (AA); area accumulation ratio (AAR) with ratios of 0.4, 0.5 and 0.6; and toe-headwall accumulation ratio (THAR) with ratios of 0.4 and 0.5; Benn *et al.* 2005). This approach has been successfully applied in Ladakh, northern India (Dortch *et al.*, 2010; Orr *et al.*, 2017, 2018; Saha *et al.*, 2018) and the Karakoram (Seong *et al.*, 2007), reflecting accurate estimates of the ELAs. Our study adopts methods strongly recommended by Porter (2000), whereby the mean ELA of a glacial stage also provides an estimation of the snowline altitude (SA). The aim of reconstructing ELA and SAs is to evaluate the effect of the timing and nature of glaciation on the rates of rockwall slope erosion throughout the last glacial.

Medial Moraine Descriptions

Gangotri glacier system has six major medial moraines on its surface; the three investigated moraines of this study (SD$_{A-C}$) extend over 50% of the length of the glaciers' ablation zones

(Figures 2 and 3; Table I). The medial moraines are composed of supraglacial diamict, and like many alpine glaciers, the debris thickness is heterogeneous over space and time (10^1 to 10^4 years), ranging from a few millimeters to several meters thick (Owen and Derbyshire, 1989; Schroder *et al.*, 2000; Benn *et al.*, 2012; Srivastava, 2012). The widths of the moraines range from 50 to 650 m, widening towards the snout of Gangotri glacier (Figure 3; Supporting Information Item 1). The moraine morphologies are characterized by irregular surface topographies, the result of variable diamict thicknesses, and distribution and orientation of steep relief ridges, depressions and ice cliffs. This heterogeneity contributes to variations in the surface morphology, mass balance and flow velocities of the glacier (Benn and Owen, 2002; Rowan *et al.*, 2015; Swift *et al.*, 2005; Haritashya *et al.*, 2006; Hambrey *et al.*, 2008; Gibson *et al.*, 2017), in addition to affecting the glaciers' sensitivity to climatic and environmental change (Scherler *et al.*, 2011a, 2011b).

These supraglacial diamicts are composed of massive sandy boulder gravels with a finer sandy-silt matrix containing interstitial ice (Supporting Information Item 2). The diamicts are composed of biotite granite, tourmaline leucogranite, with some gneiss, mica schist and quartzite, reflecting the local bedrock (Searle *et al.*, 1999; Srivastava, 2012). The subangular to very angular boulder gravels have surfaces that range from unweathered to moderately weathered. Striations or chattermarks are not present on any particle size. Large boulders (> 2−0.25 m) are located on or slightly offset from the moraine ridges with some evidence of varnish and previous toppling. The sediment samples are composed of granites and schists, with the exception of the SD$_A$ samples that include some gneiss clasts.

Finer sediment increases with proximity to the debris–ice interface, likely as a result of sorting through rainfall and meltwater flows (Hasnain and Thayyen, 1996). These fine sediments, and evidence of frost action on pebbles−boulders, indicate active periglacial weathering processes and continued sediment
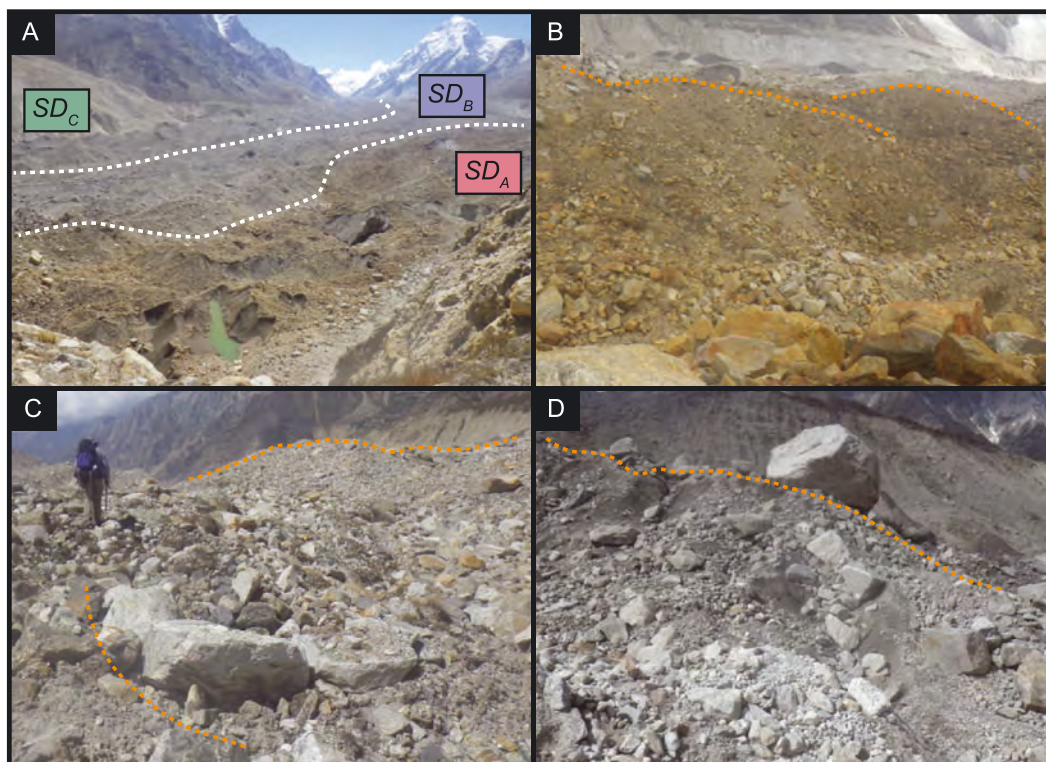

Figure 3. Views of moraines in the study area. (A) Gangotri glacier medial moraines. White and orange dashed lines highlight boundaries between moraines and moraine ridges, respectively. (B) SD$_A$ medial moraine. (C) SD$_B$ medial moraine. (D) SD$_C$ medial moraine. [Colour figure can be viewed at wileyonlinelibrary.com]

Table I. Catchment and glacier characteristics of the upper Bhagirathi catchment (uncertainties are expressed to 1σ)

	Catchment characteristics							Glacier characteristics		
Catchment	Area	Relative relief[a]	Maximum slope[b]	Mean slope[b]	Mean rockwall slope[c]	HI index[d]	[10]Be Production rate[e]	Glacier area	Glacier head	Glacier aspect
	($\sim$km^2)	(km)	(deg)	(deg)	(deg)		(at/g/a)	($\sim$km^2)	(m a.s.l.)	(deg)
Gangotri (trunk)	772.7	1.7±0.4	72	36.5±15.2	43.3±13.9	0.4	95.4±12.2	409.0	6000	330
Raktavaran	139.0	1.6±0.3	68	37.1±15.1	45.1±13.6	0.5	104.4±13.5	39.3	6280	260
Chaturangi	214.8	1.7±0.3	60	33.9±13.9	36.8±12.0	0.4	95.4±11.9	124.1	6125	270
Swachhand	39.3	1.7±0.3	57	31.2±13.8	35.3±12.1	0.4	102.8±13.3	15.1	5820	220
Maiandi	19.5	1.7±0.3	75	40.7±18.4	47.2±14.3	0.3	107.3±13.9	17.3	6000	200
Sumeru	12.3	1.4±0.4	57	29.6±15.7	32.8±12.8	0.4	90.6±11.7	12.2	5450	60
Ganohim	35.1	2.2±0.3	61	35.4±19.0	42.0±11.9	0.3	96.0±12.4	24.2	5735	45
Kirti	79.5	2.1±0.2	63	35.1±14.7	43.3±13.9	0.3	93.1±12.1	25.2	6300	45
Meru	23.6	2.0±0.3	61	37.5±18.3	45.4±12.2	0.4	87.0±11.3	8.0	5540	30

[a]A 3 km radius relative relief.
[b]Slope calculated from 0.001 km^2 catchment grid cells (map provided in Supporting Information Item 3).
[c]Slope for rockwall only, calculated from 0.001 km^2 catchment grid cells.
[d]Hypsometric Index (mean elevation – minimum elevation/relief) of Strahler (1952).
[e]Details of [10]Be production rates for catchments is provided in Supporting Information Item 3.

production and/or clast modification by interclast attrition and abrasion across the glacier surface (Owen *et al.*, 2003; Benn and Evans, 2014; Benn *et al.*, 2012). No clear englacial sediment horizons were identified in the field, despite some evidence of englacial silts and sands at the glacier surface. The exhumation of subglacial sediment to the englacial or supraglacial environments is therefore likely to be very localized (Owen *et al.*, 2003). Discontinuous soil development and tundra vegetation are restricted to the stable medial moraine ridges.

SD$_A$ moraine

The SD$_A$ medial moraine extends $\sim$12 km from the Kirti tributary catchment to within $\sim$500 m of the snout of the Gangotri glacier. A medial moraine from a Kirti sub-catchment coalesces with the main tributary moraine at 4670 m a.s.l. SD$_A$ narrows in width at the confluence ($\sim$600–300 m) between Kirti and Gangotri glaciers, as a result ice deformation and shearing (Hubbard *et al.*, 2004; Gibson *et al.*, 2017). The SD$_A$ diamict has a unique rusty brown color, likely the result of the weathering of the local Augen gneiss or Vaikrita group gneiss bedrock slopes (Figure 3B; Supporting Information Item 1). Sharing the same source outcrops, the medial moraine (SD$_E$) of Ganohim glacier also has this coloration. The G$_{sup1}$ (30.9°N, 79.09°E, 4315 m a.s.l.) was retrieved $\sim$3 km from the glacier snout. The G$_{sup2}$ (30.9°N 79.08°E) was collected at 4280 m a.s.l., $\sim$500 m downstream and northwest of G$_{sup1}$.

SD$_B$ moraine

SD$_B$ is the centermost, gray medial moraine of Gangotri glacier that extends $\sim$15 km from the modern ELA (4510–5160 m a.s.l.) to the glacier snout (Figure 3C; Supporting Information Item 1). SD$_B$ is the most stable moraine of this study, with proportionally fewer ice cliffs, ice collapse features and interstitial ice within the diamict matrix. The G$_{sup3}$ (30.89°N, 79.09°E) was retrieved at 4325 m a.s.l., $\sim$300 m northeast of G$_{sup1}$, $\sim$3 km from the glacier terminus. The G$_{sup4}$ (30.90°N, 79.09°E) was collected $\sim$500 m northwest and down glacier from G$_{sup3}$, at 4285 m a.

s.l. The G$_{sup5}$ (30.92°N, 79.08°E) was sampled $\sim$500 m from the glacier snout at 4130 m a.s.l.

SD$_C$ moraine

SD$_C$ also extends $\sim$15 km from the modern ELA to the glacier snout. The diamict has a slightly darker gray coloration to the SD$_B$ moraine (Figure 3D; Supporting Information Item 1). Due to access, only one sample could be retrieved from this moraine, $\sim$500 m from the glacier snout. The G$_{sup6}$ (30.92°N, 79.08°E) was collected at 4130 m a.s.l., slightly upstream from the confluence between the Raktavaran tributary catchment and Gangotri trunk glacier.

Results

Medial moraine sediment analysis

Gangotri and Kirti glacier medial moraine samples consist of medium-coarse sands and fine gravels; these fractions together account for 71 to 73% by weight of each sample (Figure 4). The variability in grain size distributions in the samples is insufficient to draw any conclusions about the transport and sorting of medial moraine sediment in upper Bhagirathi. No significant relationship is observed between grain size distribution and proximity of the sample to the glacier snout or margin (Supporting Information Item 2). Caution must be exercised however when interpreting shifts in grain size, or lack of, with distance down-glacier, as only three or fewer samples are collected from each moraine.

The medial moraine samples are largely made up of angular (32−48%) and subangular (19−46%) grains, with $\leq$ 1% of grains considered either rounded or well rounded (Supporting Information Item 2). Grains of low sphericity constitute between 71 and 82% of each sample. The bladed (14−23%) and very bladed (30−40%) grain shape classes are the most prevalent the samples, where over 50% of grains per sample have *c:a* and *b:a* ratios < 0.3 (Figure 5). No significant relationship can be identified between grain size and grain roundness or sphericity for any one moraine or sediment sample (Supporting Information Item 2).

The covariance of clast shape and roundness indices are presented in RA-C$_{40}$ (angular, very angular) and RWR-C$_{40}$ (rounded, well rounded) plots for Gangotri glacier and previous studies in Figure 5. Distinguishing between transport pathways must be approached with care due to the pronounced overlap in facies indices, an important consideration when working in complex alpine settings (Lukas et al., 2013). The RA (85−94%) and C$_{40}$ (75−96%) indices and large proportion of bladed and extremely bladed grains suggest that the medial moraines of this study share a supraglacial transport history (Benn and Owen, 2002; Hubbard, 2004; Lukas et al., 2013). Some extraglacial and moraine control samples also record RA values greater than 80%. The RWR indices for the medial moraines range between 6 and 15%, higher than the ~0% values typical for supraglacial samples. The more rounded component of the samples may reflect the input of sediment from other realms of the glacial system, clast rounding by englacial and/or supraglacial transport, or the effects of meltwater on the glacier surface.

Percentage surface weathering estimates of quartz grains range from 30 to 100%, with mean surface weathering for the samples ranging between 66 ± 22 to 78 ± 17%. A slight, yet negligible increase in surface weathering can be identified down glacier for the SD$_A$ and SD$_B$ moraines, and the glacier as a whole. Further detail of these earlier-mentioned analyses and further sediment analyses that proved less significant to the conclusions of this study are provided in Supporting Information Item 2.

Rockwall slope erosion rates of the upper Bhagirathi catchment

The modeled accumulation of ^{10}Be during the transport of sediment between the source rockwall and medial moraine ranged between 0.02×10^4 and 0.025×10^4 at/g SiO$_2$ (Table II; Supporting Information Item 3). The subtraction of this ^{10}Be from the total measured ^{10}Be concentrations increases the calculated erosion rates by ~8.7 to 30.2% relative to uncorrected values.

The accumulation of ^{10}Be during transport along the moraine length is also a concern due to the high production rates (87.0 ± 11.3 to 107.3 ± 13.9 at/g/a) of upper Bhagirathi. If ^{10}Be were to accrue during this transport, G$_{sup5}$ would theoretically record a concentration at least 0.4×10^4 at/g greater than G$_{sup3}$, which is located 2.5 km up-glacier. Instead a difference of ~0.1×10^4 at/g is measured, which shows that the sampled sediment was transported down-glacier at depth in the medial moraine, permitting limited-no ^{10}Be accumulation. In order to test this assumption, the maximum accumulation of ^{10}Be along the SD$_{A-C}$ moraines was estimated used methods outlined by Seong et al. (2009; Supporting Information Item 3). The estimates exceed the total sample concentrations measured, therefore indicating little ^{10}Be production during transport along the medial moraines. This suggests that the supraglacial sediment samples were not exposed at the surface for the entire length of each landform. The collection of multiple samples per medial moraine with a known source area is therefore recommended in order to help identify samples that do not reflect the mean surface concentrations of the catchment rockwall. To reduce the potential accumulation of ^{10}Be during this transport, and its affect upon the erosion rates, this approach is perhaps best applied in catchments with medial moraines < 5 km in length, particularly in areas with high annual ^{10}Be production.

Furthermore, G$_{sup1}$ and G$_{sup2}$ from the SD$_A$ moraine have ^{10}Be concentrations of 1.1 ± 0.2 and 1.6 ± 0.3 × 10^4 at/g

SiO$_2$, respectively. These concentrations infer rockwall slope erosion rates of 6.9 ± 1.9 mm/a for the G$_{sup1}$ sample, and 4.3 ± 1.1 mm/a for G$_{sup2}$ (Table II). The G$_{sup3}$, G$_{sup4}$, and G$_{sup5}$ samples from the SD$_B$ moraine have ^{10}Be concentrations of 2.7 ± 0.3, 2.5 ± 0.3 and 2.6 ± 0.3 × 10^4 at/g SiO$_2$ respectively. An inferred erosion rate of 2.4 ± 0.4 mm/a is derived from G$_{sup3}$, 2.5 ± 0.5 mm/a from G$_{sup4}$, and 2.4 ± 0.4 mm/a from G$_{sup5}$. The SD$_C$ G$_{sup6}$ sample has a ^{10}Be concentration of 1.5 ± 0.4 × 10^4 at/g SiO$_2$ and an inferred slope erosion rate of 4.3 ± 1.4 mm/a.

Topographic and geomorphic analyses

The detailed geomorphic mapping of upper Bhagirathi revealed that the identification of discrete geomorphic zones within the catchment is not possible owing to the absence of the vertical stratification of landforms (Figure 2; Supporting Information Item 4). River terraces and fans occupy elevations < 5000 m a.s.l., whereas the remaining landforms extend the full extent of the catchment.

The slopes of upper Bhagirathi catchment range from 0° to 75°, gentle (< 30°), moderate (31°−45°) and steep (> 46°) slopes occupying 38, 25 and 37% of the total catchment, respectively. The mean tributary catchment slopes of the study area range between 29.6 ± 15.7 and 40.7 ± 18.4° (Table I). Between 10 and 53% of the catchment areas are occupied by glaciers; the glacier surface slopes are included within this catchment slope analysis, which introduces a degree of uncertainty to these mean slope values. Catchment 3-km-radius relief ranges from 1.4 ± 0.4 to 2.2 ± 0.3 km.

Steep relief slopes that exceed 35° are largely unable to support regolith, snow or ice (Gruber and Haerberli, 2007; Nagai et al., 2013). The mean slopes of the rockwalls range between 32.8° ± 12.8° and 47.2° ± 14.3° (Table I). Srivastava (2012) maintains that ~50% of the catchment's rockwall slopes have angles > 60°. The steep topography of the catchment therefore means that it is susceptible to both rockfall and avalanching (Hewitt, 1988; Bookhagen et al., 2005; Dunning et al., 2007; Gruber and Haerberli, 2007; Mitchell et al., 2007), which likely provides the primary source of supraglacial sediment to Gangotri and Kirti glaciers (Srivastava, 2012).

Ideal conditions for periglacial weathering processes including frost-shattering, cryofracturing, and frost heave are present throughout the upper Bhagirathi catchment. Optimum frost cracking conditions (-3 to -8°C) within the catchment migrate from elevations of ~5680−6380 m a.s.l. during the summer, to ~3780−4480 m a.s.l. during the winter (Figure 6A). This is consistent with the frost-cracking envelope between 4000−6000 m a.s.l. devised by Brozović et al. (1997) for the NW Himalaya. These temperatures extend to a maximum depth of ~2.3 m into the near-surface, between 3780 and 4430 m a.s.l. (Figure 6B).

Peaks which exceed ~6380 m a.s.l. (including Shivling, Meru and the Chaukhamba Massif) have surface temperatures < -8° C, which theoretically reduces the efficiency of periglacial weathering processes. The distribution and magnitude of these processes are affected by diurnal and seasonal cycles and climatic and microclimatic variations. Optimum frost cracking conditions over the last few glacial cycles are likely to have extended to lower and higher elevations within the catchment than the present.

Transient or seasonal permafrost can occur at elevations between 3380 and 5280 m a.s.l. within upper Bhagirathi; at higher elevations the permafrost can be permanent. Transient permafrost, which exacerbates slope instabilities and mass wasting (Fischer et al., 2006), may extend from the catchment

slopes to the proglacial zone of Gangotri glacier and catchment floor. Permafrost penetrates the near surface between 3080 and 3380 m a.s.l., to a maximum depth of ~0.8 m (Figure 6B).

ELA and SA reconstructions

The ELAs of contemporary glaciers range from 4880 to 5665 m a.s.l. (Table III), falling within the uncertainties of, and marginally above past estimates of 4510 to 5390 m a.s.l. (Owen and Sharma, 1998; Naithani *et al.*, 2001; Ahmad *et al.*, 2004, Burbank *et al.*, 2003; Srivastava, 2012; Singh *et al.*, 2017). Gangotri glacier has retreated ~30 km upstream over the past ~60 ka (Owen and Sharma, 1998; Burbank *et al.*, 2003), the ELA rising in elevation from 4095 ± 295 to 5160 ± 160 m a.s. l., providing an ΔELA of 1065 ± 295 m. Glacial studies across the Tethyan Himalaya of northern India (Dortch *et al.*, 2011; Orr *et al.*, 2017, 2018) and the Tibetan plateau (Heyman, 2014) document maximum ΔELAs between 240−290 and 280−494 m, respectively; the magnitude of Gangotri glacier retreat over this timescale stands in stark contrast to these. This rate of recession has yet to be determined in Garhwal, where local glacial stages record ΔELAs < 100 m within the past 1 ka, compared to an ΔELA of 465 ± 100 m for Gangotri glacier. A net loss in glacier volume since 1.6 ka is indicated by the heights of the ice-contact Gangotri glacial stage moraines relative to the glacier surface. Approximately 50% of the total catchment is above the modern snowline altitude (5160 ± 160 m a.s.l.).

Discussion

Bhagirathi rockwall slope erosion

Medial moraine sediment characteristics for the lower ~3 km of the ablation zone of Gangotri glacier are broadly similar, despite the discrete origins of each landform. Grain shape analysis indicates a predominantly supraglacial transport history with possible contributions from other landscape realms, i.e. moraine, extraglacial sources (hillslope deposits). Grain roundness and surface weathering is attributed to periglacial weathering

Figure 4. Particle size distribution of Gangotri medial moraine samples. [Colour figure can be viewed at wileyonlinelibrary.com]

processes including freeze–thaw, frost cracking and ice wedging, which dislodge angular rock fragments from the bedrock and/or regolith slopes (Benn and Lehmkuhl, 2000; Schroder *et al.*, 2000; Benn *et al.*, 2003; Hambrey *et al.*, 2008; Lukas *et al.*, 2012).

Moisture availability, surface temperature (Hales and Roering, 2007; Humphreys and Wilkinson, 2007; Moores *et al.*, 2008; Dühnforth *et al.*, 2010; Fischer *et al.*, 2010, 2012; West *et al.*, 2014; Eppes and Keanini, 2017) and rock mass strength (Augustinus, 1995; Wegmann *et al.*, 1998; Murton *et al.*, 2006; Eppes and McFadden, 2008) are likely to moderate the rockwall debris flux and influence the derived slope erosion rates of this study. In summary, the steep relief topography of the upper Bhagirathi catchment in conjunction with optimal surface temperatures for periglacial erosion promotes slope–glacier coupling through mass wasting events including rockfalls and avalanching (Brozović *et al.*, 1997; Anderson, 2005; Matsuoka and Murton, 2008; Foster *et al.*, 2010; Scherler *et al.*, 2011b). Rockfalls therefore play a significant, if not principal role in rockwall slope erosion, which is consistent with the observation that mass movements are a dominant mechanism for Himalayan landscape denudation (Gabet *et al.*, 2004; Dortch *et al.*, 2009; Lupker *et al.*, 2012). The frequency and magnitude of rockfall events over 10^3–10^5 year timescales are likely controlled by regional erosion rates, which are moderated by climate and/or tectonism (Molnar *et al.*, 2007; Scherler *et al.*, 2014; Gibson *et al.*, 2017).

The ^{10}Be concentrations vary between the samples of each moraine of Gangotri glacier and between individual landforms, despite sharing similar sediment characteristics (Figure 7; Table II). No relationship is evident between ^{10}Be concentration and distance down-glacier or proximity to the glacier margin. The range in ^{10}Be concentrations of our dataset (1.1 ± 0.2 × 10^4 to 2.7 ± 0.3 × 10^4 at/g SiO_2) may be due to variability in the timing and magnitude of mass wasting events, the insufficient mixing of sediment, the prior or punctuated exposure to cosmic rays, and shielding by snow, ice or regolith (Seong *et al.*, 2009; Ward and Anderson, 2011; Heyman *et al.*, 2011).

The SD_A moraine records the lowest ^{10}Be concentrations (1.1 ± 0.2 × 10^4 to 1.6 ± 0.3 × 10^4 at/g SiO_2), corresponding to the highest inferred slope erosion rates of this study (4.3 ± 1.1 to 6.9 ± 1.9 mm/a). The close proximity of SD_A to rockwall slopes and external sediment sources along the length of the landform, and the possible greater sensitivity of smaller catchments to external forcing, are two possible explanations for these lower TCN concentrations. The concentration disparity between the SD_A samples may due to the sampling of isolated rockfall event(s) rather than amalgamated moraine sediment. Similarly, the sedimentology and low ^{10}Be concentrations of SD_C G_{sup6} may be the result of sediment input from proximal rockwall slopes at the snout of Gangotri glacier or contributions from Raktavaran and/or Chaturangi tributary glaciers.

The SD_B samples have the highest ^{10}Be concentrations of this study (2.5 ± 0.3 × 10^4 to 2.7 ± 0.3 × 10^4 at/g SiO_2), which each fall within uncertainty of each other, and record the lowest inferred slope erosion rates (2.4 ± 0.4 to 2.5 ± 0.5 mm/a). The SD_B moraine extends the full length of the ablation zone of Gangotri glacier with no direct contact with the catchment slopes. Accordingly, the SD_B rates are considered to be the most representative of upper Bhagirathi rockwall slope erosion, and likely captures the background erosion rates of the periglacial realms of the catchment due to mass wasting. The SD_B erosion rates are therefore likely to be largely dictated by high frequency, low magnitude mass wasting events, while the SD_A and SD_C signals are controlled by large stochastic events. These SD_B rates affirm that ~2.5 m of lateral slope erosion through periglacial processes can be achieved across a
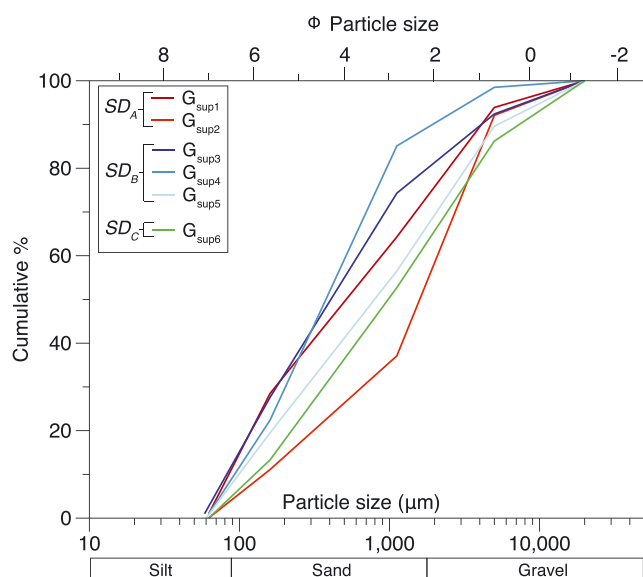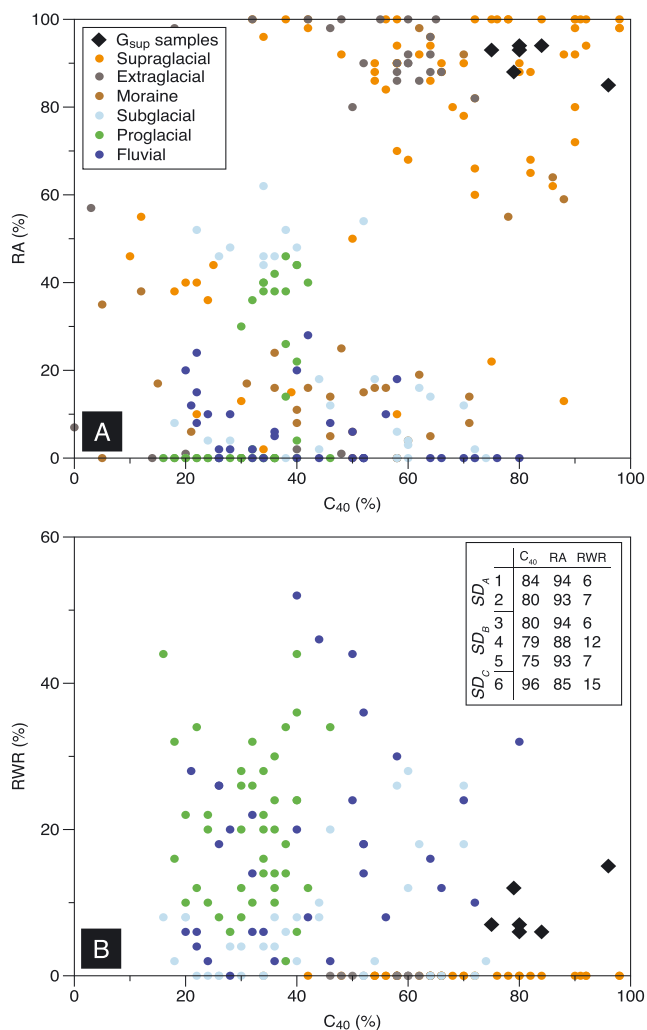
Figure 5. Covariance plots of medial moraine samples from Gangotri glacier with a compilation of sediment samples from high altitude alpine catchments. Batal (Benn and Owen, 2002), Khumbu (Hambrey *et al.*, 2008), d'Arolla (Goodsell *et al.*, 2005) and Findelen, Pasterze, Estelette, Tasman, Vadret and Fox glaciers (Lukas *et al.*, 2013). (A) Plot of RA-C_{40} index, (B) RWR-C_{40} index. [Colour figure can be viewed at wileyonlinelibrary.com]

single millennium in this catchment, and > 65 m when extrapolated for the whole of the Holocene. To test the robustness of our interpretations, it would be worthwhile to extend this investigation up-glacier and evaluate variations in ^{10}Be concentrations throughout the ablation zone, and across grain sizes.

The ELA reconstructions for the local glacial stages show that the size of the glacier and the spatial extent of the periglacial realms has decreased over the last 60 ka (Table III). This means that the slope area contributing debris directly to the accumulation zones of the glaciers have reduced, alongside the contribution of glacial erosion to the debuttressing of slopes.

Studies suggest that the timing and nature of glaciation and the associated geomorphic change for the upper Bhagirathi catchment is primarily governed by climate (Barnard *et al.*, 2004a, 2004b; Srivastava, 2012; Singh *et al.*, 2017). The magnitude and rates of rockwall slope erosion are therefore not only intrinsically linked to climate through periglacial weathering processes, but also as a result of climate-driven glaciation affecting the extent of slope–glacier coupling. Accordingly, rates of rockwall slope erosion and the contribution of the periglacial realms to the denudation budget of the catchment is likely to have fluctuated throughout the last glacial.

Garhwal landscape denudation

Scherler *et al.* (2015) have shown that rates of fluvial incision in Garhwal during the late Pleistocene was greater than the present by a factor of ~2 to 4. Whether periglacial erosion has remained constant or varied across these timescales, the influence of rockwall slope erosion on the topographic evolution of upper Bhagirathi is likely to have been maintained over time. The magnitude of this erosion is likely to affect sediment flux and the storage of snow and ice from diurnal to millennial timescales in this setting, and then more broadly influence catchment configuration and margin migration, microclimates (Bhambri *et al.*, 2011; Srivastava, 2012), and be sufficient to limit relief and affect the architectural organization of the local fault systems (Valdiya, 1991; Sorkhabi *et al.*, 1996; Bali *et al.*, 2003). The frequency and magnitude of rockfall events in Bhagirathi is therefore likely to be affected, in part, by catchment-specific conditions such as geologic setting and geomorphic regime, and then external forcing such as shifts in climate or tectonism. The global intensification of late Pleistocene glaciation, for example, caused extensive mass redistribution and localized incision throughout the Himalayan-Tibetan orogen (Zeitler *et al.*, 2001; Brozović *et al.*, 1997; Bookhagen *et al.*, 2005; Hewitt, 2009; Whipple, 2009). This is likely to be similar in the Bhagirathi catchment where landscape denudation can be attributed to a changing glacier mass balance over time.

Comparing lateral slope erosion with other records of landscape change is a challenge as they invariably reflect erosion or denudation through a variety of mechanisms and across different temporal and spatial scales. Moreover, TCN derived catchment-wide erosion rates reflect the net surface lowering of a catchment, which accounts for both vertical and lateral erosion. Similarly, rates of exhumation defined using low temperature thermochronology describe the ascension of rock through modeled isotherms. To better compare our dataset with these records, we calculate an approximate vertical component to our slope erosion data (Table II). Overall the rates of rockwall slope erosion largely exceed the averaged catchment-wide erosion and exhumation rates of upper Bhagirathi and the Garhwal region (Figure 7). Our erosion dataset supports the view that slope erosion of alpine headwaters can outpace the wider drainage basin (Oskin and Burbank, 2005; Naylor and Gabet, 2007), and that the distribution and magnitude of erosion can vary significantly over short distances downstream (Scherler *et al.*, 2014). The difference in the rates of erosion and landscape denudation between these various records may be because our slope erosion dataset offers a higher resolution record of erosion ($10^1 - 10^4$ years) than those on the catchment or mountain range scale ($10^4 - 10^6$ years) and/or that these latter records eliminate the 'noise' in sediment flux data over time, such as single mass wasting events initiated by large and/or stochastic seismic events (Sadler and Jerolmack, 2014; Willenbring *et al.*, 2013). The slope erosion rates of this study remain largely lower than the regional uplift rates of 4 to 5.7 mm/a (Barnard *et al.*, 2004a, 2004b; Scherler *et al.*, 2014), which may explain the preservation of high relief slopes within the study area.

Rockwall slope erosion of the NW Himalaya

Comparisons between ^{10}Be concentrations in medial moraine sediment of the Bhagirathi glaciers with similar datasets from Chhota Shigri in Lahul (Scherler and Egholm, 2017) and Baltoro glacier in the Central Karakoram (Seong *et al.*, 2009) show that the ^{10}Be concentrations at these other localities exceed those in our study (Figure 8). The SD_B samples that are considered to

Table II. Medial moraine sample AMS ratios, [10]Be concentrations and inferred slope erosion rates for the upper Bhagirathi catchment

Sample	Moraine	Location Latitude (°N)	Longitude (°E)	Elevation (m a.s.l.)	[10]Be production rate[a] (at/g SiO$_2$/a)	Quartz mass (g)	[9]Be carrier mass,conc. (g, mg/g)	Cosmogenic [10]Be data AMS [10]Be/[9]Be ratio[b] (10^{-15})	[10]Be concentration (10^4 at/g)	[10]Be accum. transport[c] (10^4 at/g)	Lateral slope erosion rate Erosion rate[d] (mm/a)	Adjusted erosion rate[e] (mm/a)	Applicable time range[f] (ka)	Vertical erosion Inferred erosion rate[g] (~mm/a)
Kirti														
G$_{sup1}$	SD$_A$	30.90	79.09	4315	93.1±12.1	18.7000	0.2631, 1.041	13.7±2.5	1.1±0.2	0.025	5.3±1.2	6.9±1.9	0.09	5.0
G$_{sup2}$	SD$_A$	30.90	79.08	4280	93.1±12.1	18.7000	0.2563, 1.041	19.2±3.4	1.6±0.3	0.025	3.6±0.8	4.3±1.1	0.14	3.1
Gangotri														
G$_{sup3}$	SD$_B$	30.89	79.09	4325	95.4±12.2	18.6000	0.2586, 1.041	30.2±3.5	2.7±0.3	0.020	2.1±0.4	2.4±0.4	0.25	1.7
G$_{sup4}$	SD$_B$	30.90	79.09	4285	95.4±12.2	14.6000	0.2652, 1.041	22.6±2.8	2.5±0.3	0.020	2.3±0.4	2.5±0.5	0.24	1.8
G$_{sup5}$	SD$_B$	30.92	79.08	4130	95.4±12.2	16.4000	0.2634, 1.041	25.8±3.1	2.6±0.3	0.020	2.2±0.4	2.4±0.4	0.25	1.7
G$_{sup6}$	SD$_C$	30.92	79.08	4130	95.4±12.2	19.9000	0.2550, 1.041	19.8±5.3	1.5±0.4	0.020	3.8±1.1	4.3±1.4	0.14	3.1

[a]Mean catchment production rates calculated using methods described in Dortch et al. (2011).
[b][10]Be/[9]Be ratios are corrected for background [10]Be detected in procedural blank (0.3 ± 0.1 × 10^{-14}). Negligible (< 1 ppm) [9]Be was detected in each sample.
[c]Accumulation of [10]Be during burial, englacial transport and exhumation is calculated using methods detailed in Ward and Anderson (2011; see Supporting Information Item 3).
[d]Erosion rate which does not include [10]Be accumulation during transport from source bedrock slope to medial moraine. [10]Be decay constant of 5.1 ± 0.3 × 10^{-7}, and a [10]Be half-life of 1.36 Ma.
[e]Erosion rate which has been adjusted for [10]Be accumulation during transport from source bedrock slope to medial moraine.
[f]Applicable time range follows Lal (1991).
[g]Inferred vertical erosion: cos (mean rockwall slope) × lateral slope erosion (Heimsath and McGlynn, 2008). Mean rockwall slope: 43.3° ± 13.9°.
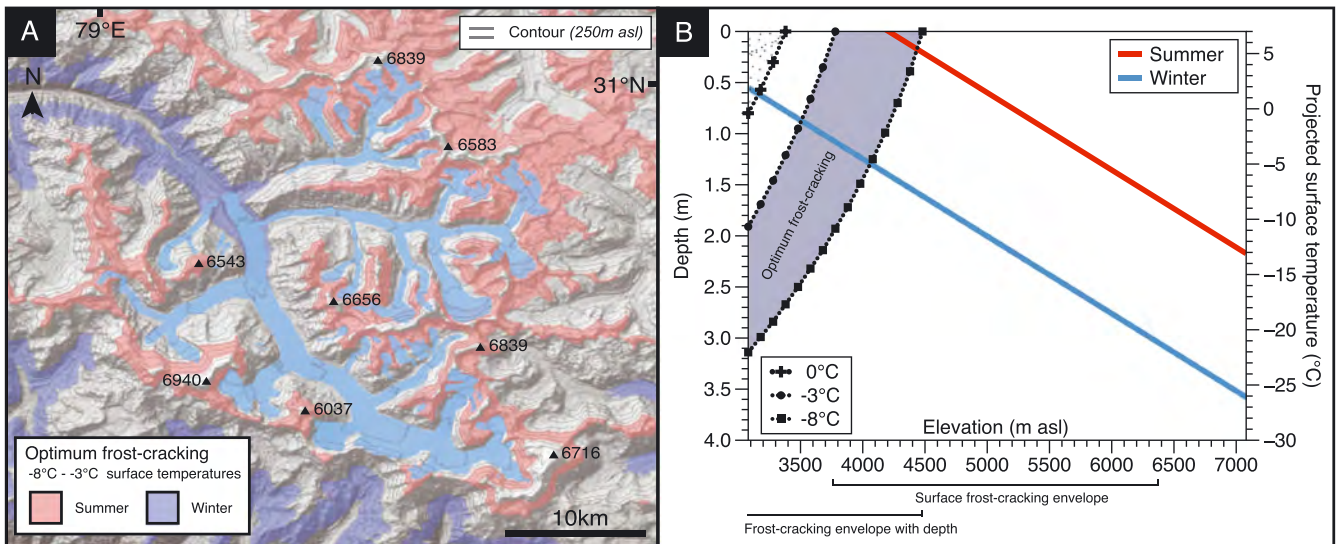
Figure 6. Optimum frost-cracking for the upper Bhagirathi catchment. (A) Simplified map showing the regional distribution of the optimum frost shattering elevations during the summer and winter (temperature data from Bhambri *et al.* [2011] and CRU 2.0). Gray shading refers to the optimal frost-cracking zone during the summer/winter transition. (B) Optimum frost cracking (blue shading) and permafrost boundaries with respect to depth and projected surface temperatures for the summer and winter within the basin elevations. Textured pattern represents elevations devoid of permafrost with depth. [Colour figure can be viewed at wileyonlinelibrary.com]

best reflect upper Bhagirathi slope erosion measure ^{10}Be concentrations $> 1 \times 10^4$ at/g SiO$_2$ lower than Chhota Shigri or Baltoro, and record erosion rates twice as fast. The ^{10}Be concentrations of the three study areas are compared with catchment parameters and regional climate records to decipher the possible drivers of rockwall slope erosion in the NW Himalaya.

No significant relationship is evident between catchment area and ^{10}Be concentration. The catchment area does not account for the total surface area of the source rockwall slopes, a parameter that may influence these concentrations to a greater extent. Approximately 80, 50 and 53% of the total catchment area of Bhagirathi, Chhota Shigri and Baltoro respectively, are above the ELA/SA altitudes and nourish the glaciers through snow and ice avalanching. Changes to the SA over time are likely to affect the relative abundance of exposed bedrock and regolith-covered slopes and will help to moderate the slope debris flux. Similarly, there is no correlation between ^{10}Be and glacier area, and by association, size of medial moraine.

No relationship is apparent between mean catchment or rockwall slope and ^{10}Be concentration, despite other studies being able to link these variables on a catchment scale and show that greater slope angles promote a larger debris flux (Finlayson *et al.*, 2002; Burbank *et al.*, 2003; Ouimet *et al.*, 2009; Scherler *et al.*, 2011b, 2014). Although the slopes will broadly facilitate rockfall and avalanching (Luckman, 1977; Gruber and Haeberli, 2007; Bernhardt and Schulz, 2010; Nagai *et al.*, 2013) and the eventual evacuation of sediment from the catchment, each of the investigated catchments is also able to store extensive volumes of sediment in the form of landforms and sediment deposits (Figure 2; Seong *et al.*, 2009). These landforms typically have gentler slopes, which transfer sediment to the glacier surface via diffusive creep processes (Carson and Kirkby, 1972). Not only will these stores of sediment have implications for the sediment flux of the catchments, but also they may influence the ^{10}Be concentrations measured within medial moraine sediment.

Table III. Reconstructed ELAs for the upper Bhagirathi catchment[a]

	Time	Area-altitude	Area-accumulation ratio			Toe-Headwall altitude ratio		Mean ELA[b]	ΔELA[c]
	(ka)	AA	AAR (0.4)	AAR (0.5)	AAR (0.6)	THAR (0.4)	THAR (0.5)	(m a.s.l.)	(m a.s.l.)
Contemporary glaciers									
Gangotri	—	5100	5210	5080	4960	5165	5440	5160±160	—
Raktavaran	—	5630	5790	5680	5560	5720	5620	5665±80	—
Chaturangi	—	5500	5650	5550	5430	5385	5665	5530±115	—
Swachhand	—	5290	5360	5280	5180	5325	5440	5310±85	—
Maiandi	—	5625	5730	5530	5400	5735	5885	5650±170	—
Sumeru	—	5155	5170	5130	5090	5170	5235	5160±50	—
Ganohim	—	5115	5200	5060	4920	5240	5375	5150±160	—
Kirti	—	4940	4920	4850	4770	5175	5350	5000±220	—
Meru	—	4875	5010	4870	4760	4830	4950	4880±90	—
Glacial stages									
Bhujbasa	~1.7−0.5	4770	4540	4760	4680	4615	4795	4695±100	465±100
Gangotri	~2.4−1.9	4750	4530	4750	4670	4605	4745	4675±90	485±90
Shivling	~5.2	4730	4530	4740	4650	4520	4710	4645±100	515±100
Sudarshan	21.0−16.0	4425	4700	4570	4410	4070	4360	4425±215	735±210
Bhagirathi	60.0−23.0	4025	4550	4290	3810	3770	4110	4095±295	1065±295

[a]ELAs rounded to the nearest multiple of five.
[b]± standard deviation.
[c]± standard deviation (of ΔELAs from all reconstructions).
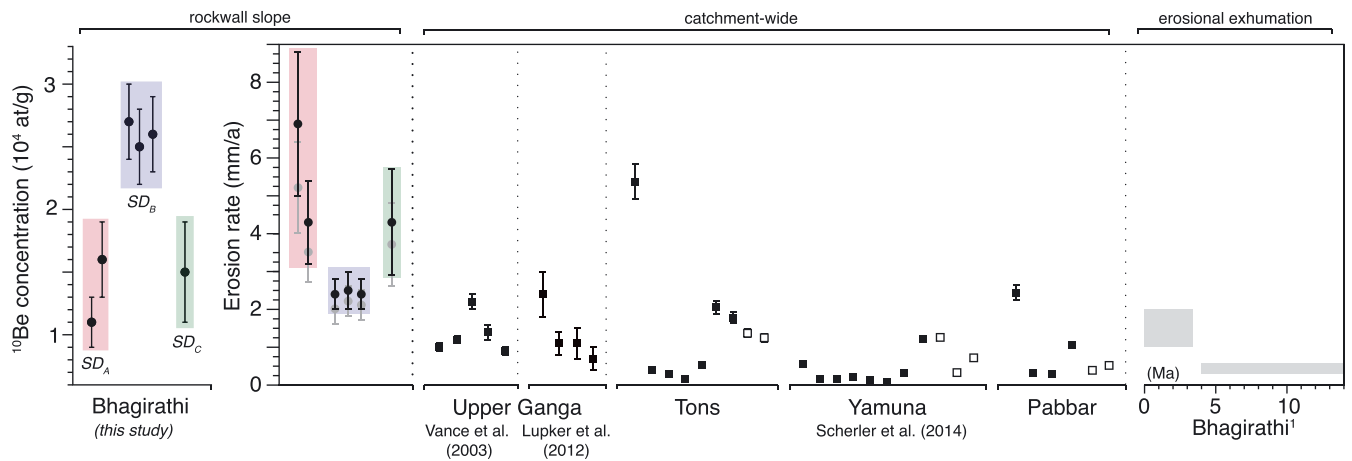
Figure 7. Beryllium-10 concentrations (10^4 at/g SiO_2) of upper Bhagirathi medial moraine samples and rates of erosion for the Garhwal Himalaya. Gray points indicate the unadjusted slope erosion rates. 1: Erosional exhumation rates using thermochronometric methods from Sorkhabi *et al.* (1996), Searle *et al.* (1999), Thiede *et al.* (2009), Thiede and Ehlers (2013). [Colour figure can be viewed at wileyonlinelibrary.com]

The 3-km-radius relief of the study areas exceed ~1.6 km, the steeper relief catchments measuring the highest ^{10}Be concentrations, and therefore the lowest inferred rockwall slope erosion rates. This suggests that rates of rockwall slope erosion can in some cases be insufficient to limit catchment relief in the NW Himalaya. A more likely explanation is that the 3-km-radius relief is largely dictated by the local uplift of the study areas.

A possible lithological control to slope erosion is expressed in upper Bhagirathi. The highest rates of erosion are defined by the SD_A and SD_C moraines, which are sourced from rockwalls composed of, in part, augen gneiss and schist respectively. Lower rates of erosion from SD_B may be due to the granitic source rockwalls that have a greater rock mass strength than those of SD_A and SD_C, and are therefore more broadly resistant to erosion (Bhattarai and Tamrakar, 2017). However, a lithological control to erosion is less clear for the NW Himalaya, where we measure a large range of ^{10}Be-derived slope erosion rates within an area argued to have a relatively uniform rock mass strength (Burbank *et al.*, 2003; Scherler *et al.*, 2014). Investigating the jointing, structure and moisture content of the catchment walls would help to evaluate the susceptibility of the rock to failure and the ongoing damage of frost action (Hallet *et al.*, 1991; Murton *et al.*, 2006; Hales and Roering, 2007).

The temperature data is recovered from weather stations outlying the study areas and therefore does not accurately reflect catchment temperatures. The ranges in annual recorded temperatures prevent any correlations being made between this climatic parameter and the derived slope erosion. The high altitude setting of each study area with mean catchment elevations > 4000 m a.s.l. (Figure 8D) does however mean that the rockwall slopes of each catchment lie within the Brozović *et al.* (1997) 4000−6000 m a.s.l. frost cracking window for the NW Himalaya.

A tentative relationship lies between mean annual rainfall and ^{10}Be concentration, where higher rainfall coincides with higher rockwall slope erosion rates. This supports the extensive work on the coupling between precipitation and erosion in the Himalaya, where enhanced moisture in the monsoon-influenced Lesser and Greater Himalaya is thought to drive more rapid landscape denudation, compared to the semi-arid interior of the orogen (Benn and Owen 1998, 2002; Harper and Humphrey, 2003; Bookhagen *et al.*, 2005; Anders *et al.*, 2006; Bookhagen and Burbank, 2006; Gabet *et al.*, 2004; Owen, 2009). This relationship is not completely straightforward for our study areas however, as ^{10}Be concentrations shared by

samples from Baltoro glacier ($4.4 \pm 0.3 \times 10^4$ to $11.7 \pm 2.2 \times 10^4$ at/g SiO_2) and Chhota Shigri (3 to 6×10^4 at/g SiO_2) receive contrasting annual rainfall of < 500 and > 900 mm, respectively. The complex climate–topography interactions of each study area prevent a conclusive relationship between erosion and this climatic parameter from being identified. This association does suggest however that rockwall slope erosion is sensitive to precipitation and therefore the glacial-periglacial realms of Himalayan catchments are likely to respond to major climatic events and/or environmental change over time.

Studies across the Himalayan-Tibetan orogen have drawn links between erosion, climate and topography (Scherler *et al.*, 2011a, 2011b, 2014; Bookhagen *et al.*, 2005; Bookhagen and Burbank, 2006; Gruber and Haeberli, 2007; Dortch *et al.*, 2011). Our regional assessment of the NW Himalaya has demonstrated that no single discussed parameter provides a dominant control for rockwall slope erosion. We must therefore consider what other variables may be influencing landscape change in these high-altitude settings.

Although glacial erosion is considered secondary to periglacial erosion; glacier dynamics may affect the rates of rockwall slope erosion. Temperate glaciers, which occupy the monsoon-influenced Himalaya, erode the glacier bed through quarrying and abrasion, which exploit fractures at the base of the catchment slopes, and also generate subglacial debris which may later be incorporated into the medial moraines (Benn and Evans, 2014; Benn and Owen, 2003). Glacier retreat and changes to mass balance can therefore lead to the debuttressing of these slopes and release glacially derived sediment. These processes can affect the rockwall debris flux and either contribute to, or trigger mass wasting (Church and Slaymaker, 1989; Watanabe *et al.*, 1998; Ballantyne, 2002a, 2002b). In the semi-arid Himalaya, sub-polar glaciers frozen to the bed are unlikely to further slope denudation processes and therefore would maintain low erosion rates. The velocity of Gangotri (< 5−120 m/a; Gantayat *et al.*, 2014; Bhattacharya *et al.*, 2016), Chhota Shigri (~20−50 m/a; Wagnon *et al.*, 2007; Azam *et al.*, 2012) and Baltoro (~30−160 m/a; Copland *et al.*, 2009) may also affect the efficiency of glacial erosion and/or influence the ^{10}Be concentrations by largely dictating the residence time of sediment on the glacier surface. Glacial hydrology and snow blow may also affect the rates of slope erosion over time (Matsuoka and Sakai, 1999, Mitchell and Montgomery, 2006; MacGregor *et al.*, 2009; Scherler *et al.*, 2011b; Barr and Spagnolo, 2015).

Studies throughout Garhwal and the NW Himalaya have underpinned a tectonic control within the distribution and

magnitude of denudation, where landscape change is strongly influenced by the Indo-Asian convergence and rock uplift patterns dictated by the geometry and shortening of the Main Himalayan Thrust (Burbank *et al.*, 2003; Thiede *et al.*, 2005; Scherler *et al.*, 2014). Although contributing to this work is beyond the scope of this study, persistent seismicity throughout the Punjab, Himachal Pradesh and Uttarkhand districts of northern India may introduce a neotectonic control to landscape evolution (Bali *et al.*, 2003; Scherler *et al.*, 2014). In Garhwal, e.g., the 1991 Uttarkashi (M 6.1; Valdiya, 1991; Owen *et al.*, 1996; Bali *et al.*, 2003) and 1999 Chamoli (M 6.6; Rajendran *et al.*, 2000) earthquakes occurred during the applicable timescales of the Bhagirathi slope erosion record and may have therefore triggered mass redistribution on a sufficient scale to affect the erosion rates of our study.

The mobilization and transfer of sediment from the catchment walls to the glacier surface is an example of one of the primary stages in the evacuation of sediment from a glacierized catchment. Models of sediment transfer on the catchment scale argue that a shift in sediment flux requires a set of preconditioning factors and one or more forcing factor (Ballantyne, 2002a, 2002b; McColl, 2012; Orr *et al.*, In press). This is true of the upper Bhagirathi catchment, where the pre-existing landscape dynamics, which include catchment parameters, and transitions in climate, tectonic or geomorphic regime, are necessary to explain the nature and rates of rockwall slope erosion over time. Understanding the topographic evolution and configuration of upper Bhagirathi and glacierized catchments throughout the NW Himalaya is made particularly challenging as it involves processes that operate across a variety of temporal and spatial scales. Despite the controls of alpine headwater evolution remaining elusive, this is the first study to quantify the rates of rockwall slope erosion in Garhwal, and has helped to demonstrate the importance of rockfall processes and the lateral erosion of slopes within mountain sedimentary systems.

Conclusion

Rockwall slope erosion has been defined for the upper Bhagirathi catchment by measuring ^{10}Be concentrations in sediment samples from three medial moraines of Gangotri glacier system. The concentrations are corrected for accumulation of ^{10}Be between the source rockwall and the medial moraine. Accumulation along the length of the medial moraines is found to be negligible. The ^{10}Be sample concentrations (1.1 ± 0.2 to 2.7 ± 0.3 × 10^4 at/g SiO$_2$) therefore reflect rates of slope erosion only. The slope erosion of the upper Bhagirathi catchment is best reflected by the SD$_B$ moraine rates, which range from 2.4 ± 0.4 to 2.5 ± 0.5 mm/a. These rates affirm that ~2.5 m of lateral slope erosion through periglacial processes can be achieved across a single millennium in this catchment, and > 65 m when extrapolated for the whole of the Holocene. Slope erosion is therefore sufficient to affect sediment flux and glacier dynamics in upper Bhagirathi, in addition to helping set the pace of topographic change at the catchment head.

The rockwall slope erosion rates (2.4±0.4–6.9±1.9 mm/a) exceed the averaged catchment-wide (0.1 ± 0.001 to 5.4 ± 0.5 mm/a; Figure 7) and erosional exhumation (1.5 ± 0.5 mm/a; Figure 7) rates of Bhagirathi and the Garhwal region, indicating that erosion at the headwaters can outpace downstream reaches and the wider catchment. A possible explanation is that the high-altitude periglacial settings of upper Bhagirathi have a greater sensitivity to external forcing such a shift in climatic conditions, than the wider catchment or mountain range. The variance found between the rates of landscape denudation may also be due to the difference in the nature and resolution of the erosion records.

Rockwall slope erosion rates are higher in upper Bhagirathi compared to the catchments of Chhota Shigri in the Lahul Himalaya and Baltoro glacier in the Central Karakoram. Comparisons were made between the erosion datasets of these three
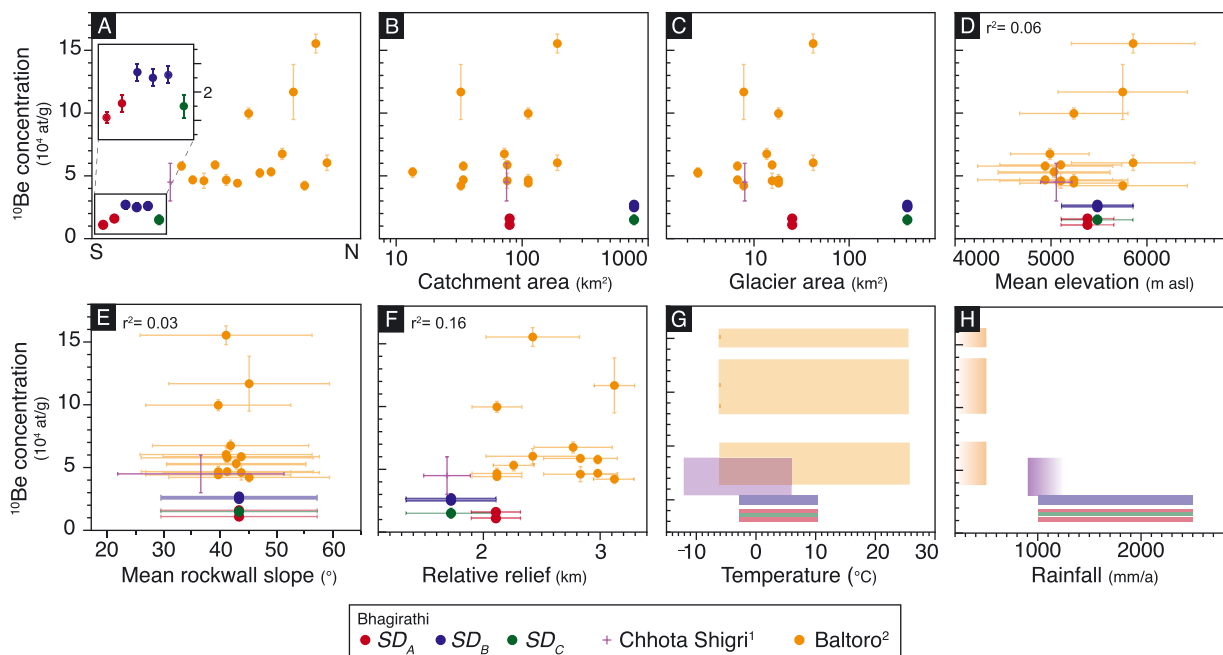

Figure 8. Comparisons between ^{10}Be concentrations (10^4 a/g SiO$_2$) for Bhagirathi, Chhota Shigri (1: Scherler and Egholm, 2017) and Baltoro (2: Seong *et al.*, 2009) glaciers (uncertainties expressed to 1σ). (A) Beryllium-10 concentrations. Inset indicates the 1σ uncertainties of the Bhagirathi samples, (B) Catchment area (r^2 value provided for all catchment data). (C) Glacier area. (D) Mean catchment elevation. (E) Mean rockwall slope (slope calculated from 0.001 km^2 catchment grid cells). (F) The 3-km-radius relief. (G) Mean annual temperature for Bhagirathi (Bhambri *et al.*, 2011), Chhota Shigri (Wagnon *et al.*, 2007) and Baltoro (Mihalcea *et al.*, 2006, 2008). (H) Annual rainfall for Bhagirathi (Bhambri *et al.*, 2011, Srivastava, 2012), Chhota Shigri and Baltoro (TRMM rainfall record [1998−2005]; Bookhagen and Burbank, 2006). [Colour figure can be viewed at wileyonlinelibrary.com]

study areas with catchment parameters and regional climate records, including catchment and glacier area, mean elevation and slope, 3-km-radius relief and annual temperature and rainfall. A tentative relationship is evident between erosion and precipitation, where more rapid slope erosion was recorded in the monsoon-influenced Lesser and Greater Himalaya, compared with the semi-arid interior of the orogen. No other individual catchment attribute was found to offer a dominant control on the rates of slope erosion in the NW Himalaya.

We were unable to confidently link rockwall slope erosion with climate-topography. We conclude that rockwall slope erosion in the three study areas and then more broadly across the NW Himalaya is likely governed by individual catchment dynamics, which vary across space and time. The frequency and magnitude of rockfall and avalanche events is therefore determined by a set of preconditioning factors unique to each catchment, and one or more local and/or regional forcing factor. By continuing to decipher the rates and controls of rockwall slope erosion, we will improve our understanding of the role and importance of periglacial processes in the morphological development of mountain ranges and contribute to future studies of sediment flux and wider landscape change across the orogen.

References

Ahmad S, Hasnain SI, Arha CD, Ramamurthy VS, Mathur KN, Bassi UK. 2004. Analysis of satellite imageries for characterization of glacio-morphological features of the Gangotri Glacier, Ganga headwater, Garhwal Himalayas. In *Proceedings of Workshop on Gangotri Glacier Special Publication Series*, Vol. **80**. Geological Survey of India: Kolkata; 61–67.

Allen T. 1981. Particle size, shape and distribution. In *Particle Size Measurement*. Springer: Boston, MA; 103–164.

Anders AM, Roe GH, Hallet B, Montgomery DR, Finnegan NJ, Putkonen J. 2006. *Spatial Patterns of Precipitation and Topography in the Himalaya*, Special Paper 398. Geological Society of America: Boulder, CO; 39.

Anderson SP. 2005. Glaciers show direct linkage between erosion rate and chemical weathering fluxes. *Geomorphology* **67**(1–2): 147–157.

Anderson RS, Anderson SP. 2010. *Geomorphology: The Mechanics and Chemistry of Landscapes*. Cambridge University Press: Cambridge.

André MF. 1997. Holocene rockwall retreat in Svalbard: a triple-rate evolution. *Earth Surface Processes and Landforms* **22**(5): 423–440.

Augustinus PC. 1995. Glacial valley cross-profile development: the influence of in situ rock stress and rock mass strength, with examples from the Southern Alps, New Zealand. *Geomorphology* **14**(2): 87–97.

Azam MF, Wagnon P, Ramanathan A, Vincent C, Sharma P, Arnaud Y, Linda A, Pottakkal JG, Chevallier P, Singh VB, Berthier E. 2012. From balance to imbalance: a shift in the dynamic behaviour of Chhota Shigri glacier, western Himalaya, India. *Journal of Glaciology* **58**(208): 315-324.

Balco G, Stone J, Lifton N, Dunai T. 2008. A complete and easily accessible means of calculating surface exposure ages or erosion rates from [10]Be and [26]Al measurements. *Quaternary Geochronology* **3**: 174–195.

Bali R, Awasthi DD, Tiwari NK. 2003. Neotectonic control on the geomorphic evolution of the Gangotri Glacier Valley, Garhwal Himalaya. *Gondwana Research* **6**(4): 829–838.

Ballantyne CK. 2002a. Paraglacial geomorphology. *Quaternary Science Reviews* **21**(18–19): 1935–2017.

Ballantyne CK. 2002b. A general model of paraglacial landscape response. *The Holocene* **12**(3): 371–376.

Ballantyne CK, Benn DI. 1994. Paraglacial slope adjustment and resedimentation following recent glacier retreat, Fåbergstølsdalen, Norway. *Arctic and Alpine Research* **26**(3): 255–269.

Barnard PL, Owen LA, Sharma MC, Finkel RC. 2001. Natural and human-induced landsliding in the Garhwal Himalaya of northern India. *Geomorphology* **40**(1–2): 21–35.

Barnard P, Owen L, Finkel R. 2004a. Style and timing of glacial and paraglacial sedimentation in a monsoon-influenced high Himalayan environment, the upper Bhagirathi Valley, Garhwal Himalaya. *Sedimentary Geology* **165**: 199–221.

Barnard PL, Owen LA, Sharma MC, Finkel RC. 2004b. Late quaternary (Holocene) landscape evolution of a monsoon-influenced high Himalayan valley, Gori Ganga, Nanda Devi, NE Garhwal. *Geomorphology* **61**(1–2): 91–110.

Barr ID, Spagnolo M. 2015. Glacial cirques as palaeoenvironmental indicators: their potential and limitations. *Earth-Science Reviews* **151**: 48–78.

Barros AP, Chiao S, Lang TJ, Burbank D, Putkonen J. 2006. *From Weather to Climate-seasonal and Interannual Variability of Storms and Implications for Erosion Processes in the Himalaya*, Special Papers 398. Geological Society of America: Boulder, CO; 17.

Bashir F, Rasul G. 2010. Estimation of water discharge from Gilgit Basin using remote sensing, GIS and runoff modeling. *Pakistan Journal of Meteorology* **6**(12): 97–113.

Benn D, Evans DJ. 2014. *Glaciers and Glaciation*. Routledge: London.

Benn DI, Lehmkuhl F. 2000. Mass balance and equilibrium-line altitudes of glaciers in high-mountain environments. *Quaternary International* **65**: 15–29.

Benn D, Owen L. 1998. The role of the Indian summer monsoon and the mid-latitude westerlies in Himalayan glaciation: a review and speculative discussion. *Journal of the Geological Society* **155**: 353–363.

Benn DI, Owen LA. 2002. Himalayan glacial sedimentary environments: a framework for reconstructing and dating former glacial extents in high mountain regions. *Quaternary International* **97–98**: 3–26.

Benn DI, Owen LA, Osmaston HA, Seltzer GO, Porter SC, Mark B. 2005. Reconstruction of equilibrium-line altitudes for tropical and sub-tropical glaciers. *Quaternary International* **138**: 8–21.

Benn DI, Kirkbride MP, Owen LA, Brazier V. 2003. Glaciated valley landsystems. *Glacial landsystems* 372–406.

Benn DI, Bolch T, Hands K, Gulley J, Luckman A, Nicholson L, Quincey D, Thompson S, Toumi R, Wiseman S. 2012. Response of debris-covered glaciers in the Mount Everest region to recent warming, and implications for outburst flood hazards. *Earth-Science Reviews* **114**(1–2): 156–174.

Bernhardt M, Schulz K. 2010. SnowSlide: a simple routine for calculating gravitational snow transport. *Geophysical Research Letters* **37**(11).

Bhambri R, Bolch T, Chaujar RK, Kulshreshtha SC. 2011. Glacier changes in the Garhwal Himalaya, India, from 1968 to 2006 based on remote sensing. *Journal of Glaciology* **57**(203): 543–556.

Bhambri R, Bolch T, Chaujar RK. 2012. Frontal recession of Gangotri Glacier, Garhwal Himalayas, from 1965 to 2006, measured through high resolution remote sensing data. *Current Science* **102**(3): 489–494.

Bhattacharya A, Bolch T, Mukherjee K, Pieczonka T, Kropacek J, Buchroithner MF. 2016. Overall recession and mass budget of Gangotri Glacier, Garhwal Himalayas, from 1965 to 2015 using remote sensing data. *Journal of Glaciology* **62**(236): 1115–1133.

Bhattarai S, Tamrakar NK. 2017. Physical Properties, Strength and Durability of Selected Rocks from the Central Nepal Lesser Himalaya, Malekhu River Area for Building Stones. *American Scientific Research Journal for Engineering*, Technology, and Sciences (ASRJETS) 35(1): 236–250.

Bierman P, Steig EJ. 1996. Estimating rates of denudation using cosmogenic isotope abundances in sediment. *Earth Surface Processes and Landforms* **21**(2): 125–139.

Biswas S, Coutand I, Grujic D, Hager C, Stöckli D, Grasemann B. 2007. Exhumation and uplift of the Shillong plateau and its influence on the eastern Himalayas: new constraints from apatite and zircon (U-Th-[Sm])/He and apatite fission track analyses. *Tectonics* **26**(6).

Bookhagen B, Burbank D. 2006. Topography, relief and TRMM-derived rainfall variations along the Himalaya. *Geophysical Research Letters* **33**: 105–109.

Bookhagen B, Thiede R, Strecker M. 2005. Late Quaternary intensified monsoon phases control landscape evolution in the northwest Himalaya. *Geology* **33**(1): 149–152.

Braucher R, Brown ET, Bourlès DL, Colin F. 2003. *In situ* produced [10]Be measurements at great depths: implications for production rates by fast muons. *Earth and Planetary Science Letters* **211**(3–4): 251–258.

Brocklehurst SH, Whipple KX. 2006. Assessing the relative efficiency of fluvial and glacial erosion through simulation of fluvial landscapes. *Geomorphology* **75**(3–4): 283–299.

Brown RJ. 1970. *Permafrost in Canada: Its Influence on Northern Development*. University of Toronto Press: Toronto.

Brown ET, Stallard RF, Larsen MC, Raisbeck GM, Yiou F. 1995. Denudation rates determined from the accumulation of in situ-produced [10]Be in the Luquillo Experimental Forest, Puerto Rico. *Earth and Planetary Science Letters* **129**(1–4): 193–202.

Brozović N, Burbank DW, Meigs AJ. 1997. Climatic limits on landscape development in the northwestern Himalaya. *Science* **276**: 571–574.

Burbank D, Blythe A, Putkonen J, Pratt-Sitaula B, Gabet E, Oskin M, Barros A, Ojha T. 2003. Decoupling of erosion and precipitation in the Himalayas. *Nature* **426**: 652–655.

Carson MA, Kirkby MJ. 1972. *Hillslope Form and Process*. Cambridge University Press: Cambridge.

Copland L, Pope S, Bishop MP, Shroder JF, Clendon P, Bush A, Kamp U, Seong YB, Owen LA. 2009. Glacier velocities across the central Karakoram. *Annals of Glaciology* **50**(52): 41–49.

Chen PY. 1977. *Table of key lines in X-ray powder diffraction patterns of minerals in clays and associated rocks*. Department of Natural Resources, Geological Survey Occasional Paper 21. Indiana Geological Survey, Bloomington.

Church M, Slaymaker O. 1989. Disequilibrium of Holocene sediment yield in glaciated British Columbia. *Nature* **337**(6206): 452.

Curry AM, Morris CJ. 2004. Lateglacial and Holocene talus slope development and rockwall retreat on Mynydd Du, UK. *Geomorphology* **58**(1-4): 85–106.

Craddock WH, Burbank DW, Bookhagen B, Gabet EJ. 2007. Bedrock channel geometry along an orographic rainfall gradient in the upper Marsyandi River valley in central Nepal. *Journal of Geophysical Research - Earth Surface* **112**(F3): 1–17.

Derbyshire E, Shi Y, Li J, Zheng B, Li S, Wang J. 1991. Quaternary glaciation of Tibet: the geological evidence. *Quaternary Science Reviews* **10**: 485–510.

De Scally FA. 1997. Deriving lapse rates of slope air temperature for meltwater runoff modeling in subtropical mountains: an example from the Punjab Himalaya, Pakistan. *Mountain Research and Development* **17**(4): 353–362.

Deeken A, Thiede RC, Sobel ER, Hourigan JK, Strecker MR. 2011. Exhumational variability within the Himalaya of northwest India. *Earth and Planetary Science Letters* **305**(1–2): 103–114.

Dortch JM, Owen LA, Haneberg WC, Caffee MW, Dietsch C, Kamp U. 2009. Nature and timing of mega-landslides in northern India. *Quaternary Science Reviews* **28**: 1037–1056.

Dortch J, Owen L, Caffee M. 2010. Quaternary glaciation in the Nubra and Shyok valley confluence, northernmost Ladakh, India. *Quaternary Research* **74**: 132–144.

Dortch J, Owen L, Schoenbohm L, Caffee M. 2011. Asymmetrical erosion and morphological development of the central Ladakh Range, northern India. *Geomorphology* **135**: 167–180.

Dühnforth M, Anderson RS, Ward D, Stock GM. 2010. Bedrock fracture control of glacial erosion processes and rates. *Geology* **38**(5): 423–426.

Dunning SA, Mitchell WA, Rosser NJ, Petley DN. 2007. The Hattian Bala rock avalanche and associated landslides triggered by the Kashmir Earthquake of 8 October 2005. *Engineering Geology* **93**(3–4): 130–144.

Dunning SA, Rosser NJ, McColl ST, Reznichenko NV. 2015. Rapid sequestration of rock avalanche deposits within glaciers. *Nature communications* **6**: 7964.

Dutta SS, Sangewar CV, Shukla SP, Chitranshi A, Puri VMK, Hampaiah P. 2004. *Some observation on physiography and geomorphology of Gangotri glacier area, Bhagirathi basin, Uttaranchal*. Geological Survey of India Special Publication 80. Geological Survey of India: Kolkata; 69–78.

Eppes MC, McFadden L. 2008. The influence of bedrock weathering on the response of drainage basins and associated alluvial fans to Holocene climates, San Bernardino Mountains, California, USA. *The Holocene* **18**(6): 895–905.

Eppes MC, Keanini R. 2017. Mechanical weathering and rock erosion by climate-dependent subcritical cracking. *Reviews of Geophysics* **55**: 470–508.

Fame ML, Owen LA, Spotila JA, Dortch JM, Caffee MW. 2018. Tracking paraglacial sediment with cosmogenic 10 Be using an example from the northwest Scottish Highlands. *Quaternary Science Reviews* **182**: 20–36.

Finkel R, Owen L, Barnard P, Caffee M. 2003. Beryllium-10 dating of Mount Everest moraines indicates a strong monsoon influence and glacial synchroneity throughout the Himalaya. *Geology* **31**(6): 561–564.

Finlayson DP, Montgomery DR, Hallet B. 2002. Spatial coincidence of rapid inferred erosion with young metamorphic massifs in the Himalayas. *Geology* **30**(3): 219–222.

Fischer L, Kääb A, Huggel C, Noetzli J. 2006. Geology, glacier retreat and permafrost degradation as controlling factors of slope instabilities in a high-mountain rock wall: the Monte Rosa east face. *Natural Hazards and Earth System Sciences* **6**(5): 761–772.

Fischer L, Amann F, Moore JR, Huggel C. 2010. Assessment of periglacial slope stability for the 1988 Tschierva rock avalanche (Piz Morteratsch, Switzerland). *Engineering Geology* **116**(1–2): 32–43.

Fischer L, Purves RS, Huggel C, Noetzli J, Haeberli W. 2012. On the influence of topographic, geological and cryospheric factors on rock avalanches and rockfalls in high-mountain areas. *Natural Hazards and Earth System Sciences* **12**(1): 241.

Foster D, Brocklehurst SH, Gawthorpe RL. 2008. Small valley glaciers and the effectiveness of the glacial buzzsaw in the northern Basin and Range, USA. *Geomorphology* **102**(3–4): 624–639.

Foster D, Brocklehurst SH, Gawthorpe RL. 2010. Glacial-topographic interactions in the Teton Range, Wyoming. *Journal of Geophysical Research - Earth Surface* **115**(F1): 1–20.

Frey H, Paul F, Strozzi T. 2012. Compilation of a glacier inventory for the western Himalayas from satellite data: methods, challenges, and results. *Remote Sensing of Environment* **124**: 832–843.

Gabet EJ, Burbank DW, Pratt-Sitaula B, Putkonen J, Bookhagen B. 2008. Modern erosion rates in the High Himalayas of Nepal. *Earth and Planetary Science Letters* **267**(3–4): 482–494.

Gabet EJ, Burbank DW, Putkonen JK, Pratt-Sitaula BA, Ojha T. 2004. Rainfall thresholds for landsliding in the Himalayas of Nepal. *Geomorphology* **63**(3–4): 131–143.

Gale SJ, Hoare PG. 1991. *Quaternary Sediments: Petrographic Methods for the Study of Unlithified Rocks*. Wiley: Chichester.

Gantayat P, Kulkarni AV, Srinivasan J. 2014. Estimation of ice thickness using surface velocities and slope: case study at Gangotri Glacier, India. *Journal of Glaciology* **60**(220): 277–282.

Gibson MJ, Glasser NF, Quincey DJ, Mayer C, Rowan AV, Irvine-Fynn TD. 2017. Temporal variations in supraglacial debris distribution on Baltoro Glacier, Karakoram between 2001 and 2012. *Geomorphology* **295**: 572–585.

Goodsell B, Hambrey MJ, Glasser NF. 2005. Debris transport in a temperate valley glacier: Haut Glacier d'Arolla, Valais, Switzerland. *Journal of Glaciology* **51**(172): 139–146.

Granger DE, Kirchner JW, Finkel R. 1996. Spatially averaged long-term erosion rates measured from in situ-produced cosmogenic nuclides in alluvial sediment. *The Journal of Geology* **104**(3): 249–257.

Gruber S, Haeberli W. 2007. Permafrost in steep bedrock slopes and its temperature-related destabilization following climate change. *Journal of Geophysical Research - Earth Surface* **112**(F2): 1–10.

Grujic D, Coutand I, Bookhagen B, Bonnet S, Blythe A, Duncan C. 2006. Climatic forcing of erosion, landscape, and tectonics in the Bhutan Himalayas. *Geology* **34**(10): 801–804.

Hales TC, Roering JJ. 2005. Climate-controlled variations in scree production, Southern Alps, New Zealand. *Geology* **33**(9): 701–704.

Hales TC, Roering JJ. 2007. Climatic controls on frost cracking and implications for the evolution of bedrock landscapes. *Journal of Geophysical Research - Earth Surface* **112**(F2): 1–14.

Hallet B, Walder JS, Stubbs CW. 1991. Weathering by segregation ice growth in microcracks at sustained subzero temperatures: verification from an experimental study using acoustic emissions. *Permafrost and Periglacial Processes* **2**(4): 283–300.

Hambrey MJ, Glasser NF. 2003. The role of folding and foliation development in the genesis of medial moraines: examples from Svalbard glaciers. *The Journal of Geology* **111**(4): 471–485.

Hambrey MJ, Quincey DJ, Glasser NF, Reynolds JM, Richardson SJ, Clemmens S. 2008. Sedimentological, geomorphological and dynamic context of debris-mantled glaciers, Mount Everest (Sagarmatha) region, Nepal. *Quaternary Science Reviews* **27**(25–26): 2361–2389.

Haritashya UK, Kumar A, Singh P. 2010. Particle size characteristics of suspended sediment transported in meltwater from the Gangotri Glacier, central Himalaya—An indicator of subglacial sediment evacuation. *Geomorphology* **122**(1-2): 140–152.

Haritashya UK, Singh P, Kumar N, Gupta RP. 2006. Suspended sediment from the Gangotri Glacier: quantification, variability and associations with discharge and air temperature. *Journal of Hydrology* **321**(1–4): 116–130.

Hasnain SI, Thayyen RJ. 1996. Sediment transport and solute variation in meltwaters of Dokriani Glacier (Bamak), Garhwal Himalaya. *Journal of the Geological Society of India* **47**(6): 731–739.

Harper JT, Humphrey NF. 2003. High altitude Himalayan climate inferred from glacial ice flux. *Geophysical Research Letters* **30**(14).

Heimsath AM, McGlynn R. 2008. Quantifying periglacial erosion in the Nepal high Himalaya. *Geomorphology* **97**(1–2): 5–23.

Hewitt K. 2009. Glacially conditioned rock-slope failures and disturbance-regime landscapes, upper Indus Basin, northern Pakistan. *Geological Society of London, Special Publication* **320**(1): 235–255.

Hewitt K. 1988. Catastrophic landslide deposits in the Karakoram Himalaya. *Science* **242**(4875): 64–67.

Heyman J. 2014. Paleoglaciation of the Tibetan Plateau and surrounding mountains based on exposure ages and ELA depression estimates. *Quaternary Science Reviews* **91**: 30–41.

Heyman J, Stroeven A, Harbor J, Caffee M. 2011. Too young or too old: evaluating cosmogenic exposure dating based on an analysis of compiled boulder exposure ages. *Earth and Planetary Science Letters* **302**: 71–80.

Hinchliffe S, Ballantyne CK. 2009. Talus structure and evolution on sandstone mountains in NW Scotland. *The Holocene* **19**(3): 477–486.

Hubbard B, Glasser N, Hambrey M, Etienne J. 2004. A sedimentological and isotopic study of the origin of supraglacial debris bands: Kongsfjorden, Svalbard. *Journal of Glaciology* **50**(169): 157–170.

Humphreys GS, Wilkinson MT. 2007. The soil production function: a brief history and its rediscovery. *Geoderma* **139**(1–2): 73–78.

Kattel DB, Yao T, Yang K, Tian L, Yang G, Joswiak D. 2013. Temperature lapse rate in complex mountain terrain on the southern slope of the central Himalayas. *Theoretical and Applied Climatology* **113**(3–4): 671–682.

Kattel DB, Yao T, Yang W, Gao Y, Tian L. 2015. Comparison of temperature lapse rates from the northern to the southern slopes of the Himalayas. *International Journal of Climatology* **35**(15): 4431–4443.

Kohl CP, Nishiizumi K. 1992. Chemical isolation of quartz for measurement of *in situ* produced cosmogenic nuclides. *Geochimica et Cosmochimica Acta* **56**: 3583–3587.

Kumar K, Miral MS, Joshi S, Pant N, Joshi V, Joshi LM. 2009. Solute dynamics of meltwater of Gangotri glacier, Garhwal Himalaya, India. *Environmental Geology* **58**(6): 1151–1159.

Lal D. 1991. Cosmic ray labelling of erosion surfaces: in situ nuclide production rates and erosion models. *Earth and Planetary Science Letters* **104**: 429–439.

Luckman BH. 1977. The geomorphic activity of snow avalanches. *Geografiska Annaler. Series A, Physical Geography* **59**(1–2): 31–48.

Lukas S, Graf A, Coray S, Schlüchter C. 2012. Genesis, stability and preservation potential of large lateral moraines of Alpine valley glaciers–towards a unifying theory based on Findelengletscher, Switzerland. *Quaternary Science Reviews* **38**: 27–48.

Lukas S, Benn DI, Boston CM, Brook M, Coray S, Evans DJ, Graf A, Kellerer-Pirklbauer A, Kirkbride MP, Krabbendam M, Lovell H. 2013. Clast shape analysis and clast transport paths in glacial environments: a critical review of methods and the role of lithology. *Earth-Science Reviews* **121**: 96–116.

Lupker M, Blard PH, Lave J, France-Lanord C, Leanni L, Puchol N, Charreau J, Bourlès D. 2012. 10Be-derived Himalayan denudation rates and sediment budgets in the Ganga basin. *Earth and Planetary Science Letters* **333**: 146–156.

MacGregor KR, Anderson RS, Waddington ED. 2009. Numerical modeling of glacial erosion and headwall processes in alpine valleys. *Geomorphology* **103**(2): 189–204.

Martin L, Blard P, Balco G, Laurent V. 2017. The CREp program and the ICE-D production rate calibration database: a fully parameterizable and updated online tool to compute cosmic-ray exposure ages. *Quaternary Geochronology* **38**: 25–49.

Matsuoka N. 2001. Microgelivation versus macrogelivation: towards bridging the gap between laboratory and field frost weathering. *Permafrost and Periglacial Processes* **12**(3): 299–313.

Matsuoka N, Murton J. 2008. Frost weathering: recent advances and future directions. *Permafrost and Periglacial Processes* **19**(2): 195–210.

Matsuoka N, Sakai H. 1999. Rockfall activity from an alpine cliff during thawing periods. *Geomorphology* **28**(3–4): 309–328.

McColl ST. 2012. Paraglacial rock-slope stability. *Geomorphology* **153**: 1–16.

Mihalcea C, Mayer C, Diolaiuti G, Lambrecht A, Smiraglia C, Tartari G. 2006. Ice ablation and meteorological conditions on the debris-covered area of Baltoro glacier, Karakoram, Pakistan. *Annals of Glaciology* **43**: 292–300.

Mihalcea C, Mayer C, Diolaiuti G, D'agata C, Smiraglia C, Lambrecht A, Vuillermoz E, Tartari G. 2008. Spatial distribution of debris thickness and melting from remote-sensing and meteorological data, at debris-covered Baltoro glacier, Karakoram, Pakistan. *Annals of Glaciology* **48**: 49–57.

Mitchell SG, Montgomery DR. 2006. Influence of a glacial buzz saw on the height and morphology of the Cascade Range in central Washington State, USA. *Quaternary Research* **65**(1): 96–107.

Mitchell WA, McSaveney MJ, Zondervan A, Kim K, Dunning SA, Taylor PJ. 2007. The Keylong Serai rock avalanche, NW Indian Himalaya: geomorphology and palaeoseismic implications. *Landslides* **4**(3): 245–254.

Molnar P, Anderson RS, Anderson SP. 2007. Tectonics, fracturing of rock, and erosion. *Journal of Geophysical Research - Earth Surface* **112**(F3): 1–12.

Montgomery DR. 2002. Valley formation by fluvial and glacial erosion. *Geology* **30**(11): 1047–1050.

Moore DM, Reynolds RC, Jr. 1997. *X-ray Diffraction and the Identification and Analysis of Clay Minerals*. Oxford University Press: Oxford.

Moore RD, Fleming SW, Menounos B, Wheate R, Fountain A, Stahl K, Holm K, Jakob M. 2009. Glacier change in western North America: influences on hydrology, geomorphic hazards and water quality. *Hydrological Processes* **23**(1): 42–61.

Moores JE, Pelletier JD, Smith PH. 2008. Crack propagation by differential insolation on desert surface clasts. *Geomorphology* **102**(3–4): 472–481.

Murton JB, Peterson R, Ozouf JC. 2006. Bedrock fracture by ice segregation in cold regions. *Science* **314**(5802): 1127–1129.

Nagai H, Fujita K, Nuimura T, Sakai A. 2013. Southwest-facing slopes control the formation of debris-covered glaciers in the Bhutan Himalaya. *The Cryosphere* **7**(4): 1303.

Naithani AK, Nainwal HC, Sati KK, Prasad C. 2001. Geomorphological evidences of retreat of the Gangotri glacier and its characteristics. *Current Science* **80**(1): 87–94.

Naylor S, Gabet EJ. 2007. Valley asymmetry and glacial versus nonglacial erosion in the Bitterroot Range, Montana, USA. *Geology* **35**(4): 375–378.

Nishiizumi K, Finkel RC, Caffee MW, Southon JR, Kohl CP, Arnold JR, Olinger CT, Poths J, Klein J. 1994. Cosmogenic production of ^{10}Be and ^{26}Al on the surface of the earth and underground. In *Eighth*

International Conference on Geochronology, Cosmochronology and Isotope Geology, US Geological Survey Circular Volume 1107. US Geological Survey: Reston, VA; 234.

Nishiizumi K, Imamura M, Caffee MW, Southon JR, Finkel RC, McAninch J. 2007. Absolute calibration of [10]Be AMS standards. Nuclear Instruments and Methods in Physics Research Section B: Beam Interactions with Materials and Atoms 258(2): 403–413.

Orr EN, Owen L, Murari M, Saha S, Caffee M. 2017. The timing and extent of Quaternary glaciation of Stok, northern Zanskar Range, Transhimalaya, of northern India. Geomorphology 284: 142–155.

Orr EN, Owen LA, Saha S, Caffee MW, Murari MK. 2018. Quaternary glaciation of the Lato Massif, Zanskar Range of the NW Himalaya. Quaternary Science Reviews 183: 140–156.

Orr EN, Owen LA, Saha S, Caffee MW. In press. Climate-driven late Quaternary fan surface abandonment in the NW Himalaya. In Ice-Age Climates-Glaciers, Floods, Lakes, and Wind: Interdisciplinary Quaternary Science Round the World to Honor Stephen C. Porter, GSA Books. The Geological Society of America: Boulder, CO.

Osmaston H. 2005. Estimates of glacier equilibrium line altitudes by the Area × Altitude, the Area × Altitude Balance Ratio and the Area × Altitude Balance Index methods and their validation. Quaternary International 138: 22–31.

Oskin M, Burbank DW. 2005. Alpine landscape evolution dominated by cirque retreat. Geology 33(12): 933–936.

Owen L. 2009. Latest Pleistocene and Holocene glacier fluctuations in the Himalaya and Tibet. Quaternary Science Reviews 28(21–22): 2150–2164.

Owen LA, Derbyshire E. 1989. The Karakoram glacial depositional system. Zeitschrift für Geomorphologie 76(Suppl): 33–73.

Owen LA, Sharma MC. 1998. Rates and magnitudes of paraglacial fan formation in the Garhwal Himalaya: implications for landscape evolution. Geomorphology 26(1–3): 171–184.

Owen LA, Sharma MC, Bigwood R. 1996. Mass movement hazard in the Garhwal Himalaya: the effects of the 20 October 1991 Garhwal earthquake and the July–August 1992 monsoon season. In Geomorphology and Land Management in a Changing Environment. Wiley: Chichester; 69–88.

Owen LA, Derbyshire E, Scott CH. 2003. Contemporary sediment production and transfer in high-altitude glaciers. Sedimentary Geology 155(1–2): 13–36.

Ouimet WB, Whipple KX, Granger DE. 2009. Beyond threshold hillslopes: channel adjustment to base-level fall in tectonically active mountain ranges. Geology 37(7): 579–582.

Placzek C, Granger DE, Matmon A, Quade J, Ryb U. 2014. Geomorphic process rates in the central Atacama Desert, Chile: insights from cosmogenic nuclides and implications for the onset of hyperaridity. American Journal of Science 314(10): 1462–1512.

Portenga EW, Bierman PR, Duncan C, Corbett LB, Kehrwald NM, Rood DH. 2015. Erosion rates of the Bhutanese Himalaya determined using in situ-produced [10]Be. Geomorphology 233: 112–126.

Porter SC. 2000. Snowline depression in the tropics during the Last Glaciation. Quaternary Science Reviews 20(10): 1067–1091.

Pratap B, Dobhal DP, Bhambri R, Mehta M. 2013. Near-surface temperature lapse rate in Dokriani Glacier catchment, Garhwal Himalaya, India. Himalayan Geology 34: 183–186.

Puri V, Srivastava D, Sangewar CV, Mukerjee B, Swaroop S. 2004. Palaeo-glaciation and glacier recession during Quaternary period in Himalaya with special reference to Bhagirathi basin, Ganga catchment. Geological Survey of India, Special Publication 80: 167–177.

Rajendran K, Rajendran CP, Jain SK, Murty CVR, Arlekar JN. 2000. The Chamoli earthquake, Garhwal Himalaya: field observations and implications for seismic hazard. Current Science (Bangalore) 78(1): 45–51.

Rowan AV, Egholm DL, Quincey DJ, Glasser NF. 2015. Modelling the feedbacks between mass balance, ice flow and debris transport to predict the response to climate change of debris-covered glaciers in the Himalaya. Earth and Planetary Science Letters 430: 427–438.

Saha S, Owen LA, Orr EN, Caffee MW. 2018. Timing and nature of Holocene glacier advances at the northwestern end of the Himalayan-Tibetan orogen. Quaternary Science Reviews 187: 177–202.

Sadler PM, Jerolmack DJ. 2014. Scaling laws for aggradation, denudation and progradation rates: the case for time-scale invariance at sediment sources and sinks. Geological Society, London, Special Publications 404: SP404–SP407.

Sanders JW, Cuffey KM, Moore JR, MacGregor KR, Kavanaugh JL. 2012. Periglacial weathering and headwall erosion in cirque glacier bergschrunds. Geology 40(9): 779–782.

Satyabala SP. 2016. Spatiotemporal variations in surface velocity of the Gangotri glacier, Garhwal Himalaya, India: study using synthetic aperture radar data. Remote Sensing of Environment 181: 151–161.

Scaillet B, Pêcher A, Rochette P, Champenois M. 1995. The Gangotri granite (Garhwal Himalaya): laccolithic emplacement in an extending collisional belt. Journal of Geophysical Research - Solid Earth 100(B1): 585–607.

Scherler D, Egholm D. 2017. Debris Supply to Mountain Glaciers and How it Effects their Sensitivity to Climate Change–A Case Study from the Chhota Shigri Glacier, India. American Geophysical Union, Fall Meeting 2017. American Geophysical Union: Washington, DC.

Scherler D, Bookhagen B, Strecker MR, von Blanckenburg F, Rood D. 2010. Timing and extent of late Quaternary glaciation in the western Himalaya constrained by [10]Be moraine dating in Garhwal, India. Quaternary Science Reviews 29(7–8): 815–831.

Scherler D, Bookhagen B, Strecker MR. 2011a. Hillslope-glacier coupling: the interplay of topography and glacial dynamics in High Asia. Journal of Geophysical Research - Earth Surface 116(F2): 1–21.

Scherler D, Bookhagen B, Strecker MR. 2011b. Spatially variable response of Himalayan glaciers to climate change affected by debris cover. Nature Geoscience 4(3): 156.

Scherler D, Bookhagen B, Strecker MR. 2014. Tectonic control on [10]Be-derived erosion rates in the Garhwal Himalaya, India. Journal of Geophysical Research - Earth Surface 119(2): 83–105.

Scherler D, Bookhagen B, Wulf H, Preusser F, Strecker MR. 2015. Increased late Pleistocene erosion rates during fluvial aggradation in the Garhwal Himalaya, northern India. Earth and Planetary Science Letters 428: 255–266.

Schroder JF, Bishop MP, Copland L, Sloan VF. 2000. Debris-covered glaciers and rock glaciers in the Nanga Parbat Himalaya, Pakistan. Geografiska Annaler. Series A, Physical Geography 82: 17–31.

Schweinfurth U. 1968. Vegetation of the Himalaya. V: Mountains and Rivers of India. In Proceedings, 21st International Geographical Congress, Calcutta, National Committee for Geography; 110–136.

Searle MP, Metcalfe RP, Rex AJ, Norry MJ. 1993. Field relations, petrogenesis and emplacement of the Bhagirathi leucogranite, Garhwal Himalaya. Geological Society, London, Special Publications 74(1): 429–444.

Searle M, Parrish R, Hodges K, Hurford A, Ayres M, Whitehouse M. 1997. Shisha Pangma Leucogranite, south Tibetan Himalaya: field relations, geochemistry, age, origin, and emplacement. Journal of Geology 150: 295–317.

Searle MP, Noble SR, Hurford AJ, Rex DC. 1999. Age of crustal melting, emplacement and exhumation history of the Shivling leucogranite, Garhwal Himalaya. Geological Magazine 136(5): 513–525.

Searle MP, Windley BF, Coward MP, Cooper DJW, Rex, AJ, Rex D, Tingdong L, Xuchang X, Jan MQ, Thakur VC, Kumar S. 1987. The closing of Tethys and the tectonics of the Himalaya. Geological Society of America Bulletin 98(6): 678–701.

Seong YB, Owen LA, Bishop MP, Bush A, Clendon P, Copland L, Finkel R, Kamp U, Shroder JF. 2007. Quaternary glacial history of the Central Karakoram. Quaternary Science Reviews 26: 3384–3405.

Seong YB, Owen LA, Caffee MW, Kamp U, Bishop MP, Bush A, Copland L, Shroder JF. 2009. Rates of basin-wide rockwall retreat in the K2 region of the central Karakoram defined by terrestrial cosmogenic nuclide [10]Be. Geomorphology 107(3–4): 254–262.

Sharma MC, Owen LA. 1996. Quaternary glacial history of NW Garhwal, central Himalayas. Quaternary Science Reviews 15(4).

Sharma P, Bourgeois M, Elmore D, Granger D, Lipschutz ME, Ma X, Miller T, Mueller K, Rickey F, Simms P, Vog S. 2000. PRIME lab AMS performance, upgrades and research applications. Nuclear Instruments and Methods in Physics Research B 172: 112–123.

Sheridan MF, Marshall JR. 1987. Comparative charts for quantitative analysis of grain textural elements on pyroclastics. In Clastic Particles, Marshall JR (ed). Van Nostrand-Reinhold: New York; 98–121.

Siddiqui MA, Maruthi KV. 2007. Detailed glaciological studies on Hamtah Glacier, Lahaul and Spiti District, HP. *Geological Survey of India* **140**: 92–93.

Singh P, Haritashya UK, Kumar N, Singh Y. 2006. Hydrological characteristics of the Gangotri glacier, central Himalayas, India. *Journal of Hydrology* **327**(1–2): 55–67.

Siewert MB, Krautblatter M, Christiansen HH, Eckerstorfer M. 2012. Arctic rockwall retreat rates estimated using laboratory-calibrated ERT measurements of talus cones in Longyeardalen, Svalbard. *Earth Surface Processes and Landforms* **37**(14): 1542-1555.

Singh P, Haritashya UK, Kumar N. 2007. Meteorological study for Gangotri Glacier and its comparison with other high altitude meteorological stations in central Himalayan region. *Hydrology Research* **38**(1): 59–77.

Singh DS, Tangri AK, Kumar D, Dubey CA, Bali R. 2017. Pattern of retreat and related morphological zones of Gangotri Glacier, Garhwal Himalaya, India. *Quaternary International* **444**: 172–181.

Sorkhabi RB, Stump E, Foland KA, Jain AK. 1996. Fission-track and $^{40}Ar^{39}Ar$ evidence for episodic denudation of the Gangotri granites in the Garhwal Higher Himalaya, India. *Tectonophysics* **260**(1–3): 187–199.

Sneed ED, Folk RL. 1958. Pebbles in the lower Colorado River, Texas a study in particle morphogenesis. *The Journal of Geology* **66**(2): 114–150.

Srivastava D. 2012. *Status Report on Gangotri Glacier. Himalayan Glaciology Technical Report, 3*. Science and Engineering Research Board, Department of Science and Technology: New Delhi; 21–25.

Strahler AN. 1952. Hypsometric (area-altitude) analysis of erosional topography. *Geological Society of America Bulletin* **63**(11): 1117–1142.

Swift DA, Nienow PW, Hoey TB. 2005. Basal sediment evacuation by subglacial meltwater: suspended sediment transport from Haut Glacier d'Arolla, Switzerland. *Earth Surface Processes and Landforms* **30**(7): 867–883.

Tangri AK. 2002. Shrinking glaciers of Uttaranchal – cause of concern – hope for the future. In *Keynote address at National Seminar on Geology and Natural Environment of Himalaya*. Nainital: 359–367.

Tangri AK, Chandra R, Yadav SKS. 2004. Temporal monitoring of the snout, equilibrium line and ablation zone of Gangotri glacier through remote sensing and GIS techniques – an attempt at deciphering the climatic variability. In *Proceedings of Workshop on Gangotri glacier*; 26–28.

Thayyen RJ, Gergan JT. 2010. Role of glaciers in watershed hydrology: a preliminary study of a "Himalayan catchment". *The Cryosphere* **4**(1): 115–128.

Thayyen RJ, Gergan JT, Dobhal DP. 2005. Slope lapse rates of temperature in Din Gad (Dokriani glacier) catchment, Garhwal Himalaya, India. *Bulletin of Glaciological Research* **22**: 31–37.

Thiede RC, Arrowsmith JR, Bookhagen B, McWilliams MO, Sobel ER, Strecker MR. 2005. From tectonically to erosionally controlled development of the Himalayan orogen. *Geology* **33**(8): 689–692.

Thiede RC, Bookhagen B, Arrowsmith JR, Sobel ER, Strecker MR. 2004. Climatic control on rapid exhumation along the southern Himalayan Front. *Earth and Planetary Science Letters* **222**(3–4): 791–806.

Thiede RC, Ehlers TA, Bookhagen B, Strecker MR. 2009. Erosional variability along the northwest Himalaya. *Journal of Geophysical Research - Earth Surface* **114**(F1): 1–19.

Thiede RC, Ehlers TA. 2013. Large spatial and temporal variations in Himalayan denudation. *Earth and Planetary Science Letters* **371**: 278–293.

Valdiya KS. 1991. The Uttarkashi earthquake of 20 October: implications and lessons. *Current Science* **61**: 801–803.

Vance D, Bickle M, Ivy-Ochs S, Kubik PW. 2003. Erosion and exhumation in the Himalaya from cosmogenic isotope inventories of river sediments. *Earth and Planetary Science Letters* **206**(3–4): 273–288.

Vannay C, Grasemann B, Rahn M, Frank W, Carter A, Baudraz V, Cosca M. 2004. Miocene to Holocene exhumation of metamorphic crustal wedges in the NW Himalaya: evidence for tectonic extrusion coupled to fluvial erosion. *Tectonics* **23**: 1–24.

Wagnon P, Lind A, Arnaud Y, Kumar R, Sharma P, Vincent C, Pottakkal JG, Berthier E, Ramanathan A, Hasnain SI, Chevallier P. 2007. Four years of mass balance on Chhota Shigri Glacier, Himachal Pradesh, India, a new benchmark glacier in the western Himalaya. *Journal of Glaciology* **53**(183): 603–611.

Ward DJ, Anderson RS. 2011. The use of ablation-dominated medial moraines as samplers for 10Be-derived erosion rates of glacier valley walls, Kichatna Mountains, AK. *Earth Surface Processes and Landforms* **36**(4): 495–512.

Watanabe T, Dali L, Shiraiwa T. 1998. Slope denudation and the supply of debris to cones in Langtang Himal, central Nepal Himalaya. *Geomorphology* **26**(1–3): 185–197.

Wegmann M, Gudmundsson GH, Haeberli W. 1998. Permafrost changes in rock walls and the retreat of Alpine glaciers: a thermal modelling approach. *Permafrost and Periglacial Processes* **9**(1): 23–33.

Wentworth CK. 1922. A scale of grade and class terms for clastic sediments. *The Journal of Geology* **30**(5): 377–392.

West N, Kirby E, Bierman P, Clarke BA. 2014. Aspect-dependent variations in regolith creep revealed by meteoric ^{10}Be. *Geology* **42**(6): 507–510.

Whipple KX. 2009. The influence of climate on the tectonic evolution of mountain belts. *Nature Geoscience* **2**(2): 97.

Whipple KX, Kirby E, Brocklehurst SH. 1999. Geomorphic limits to climate-induced increases in topographic relief. *Nature* **401**(6748): 39.

Willenbring JK, Codilean AT, McElroy B. 2013. Earth is (mostly) flat: apportionment of the flux of continental sediment over millennial time scales. *Geology* **41**(3): 343–346.

Wulf H, Bookhagen B, Scherler D. 2010. Seasonal precipitation gradients and their impact on fluvial sediment flux in the northwest Himalaya. *Geomorphology* **118**(1–2): 13–21.

Wulf H, Bookhagen B, Scherler D. 2011. Differentiating rainfall, snow and glacial melt in the Sutlej Valley (western Himalaya) by distributed hydrological modeling. *Geophysical Research Abstracts* **13**.

Zeitler PK, Koons PO, Bishop MP, Chamberlain CP, Craw D, Edwards MA, Hamidullah S, Jan MQ, Khan MA, Khattak M, Kidd WS. 2001. Crustal reworking at Nanga Parbat, Pakistan: metamorphic consequences of thermal-mechanical coupling facilitated by erosion. *Tectonics* **20**(5): 712–728.

Supporting Information

Additional supporting information may be found online in the Supporting Information section at the end of the article.

Figure S1.1. Images of the sampling locations for the investigated medial moraines of the Gangotri glacier system. White line denotes the moraine ridge.

Figure S1.2. Cross-sections of the sampling locations for the investigated medial moraines of the Gangotri glacier system.

Figure S2.1. Photomicrographs of the G_{sup4} sample from the SD_B medial moraine. A) Image of moraine surface at the G_{sup4} sampling site. B) Image of fine-coarse sand sediment fractions taken using digital microscope. C) SEM image (200x mag) of silt-clay fraction.

Figure S2.2. SEM images of Gangotri medial moraine samples. G_{sup1} i) 350x mag ii) 500x mag iii) 1000x mag. G_{sup2} i) 80x mag, ii) 350x mag, iii) 500x mag. G_{sup3} i) 120x mag, ii) 200x mag, iii) 650x mag. G_{sup4} i) 150x mag, ii) 120x mag, iii) 250x mag. G_{sup5} i) 120x mag, ii) 350x mag, iii) 500x mag. G_{sup6} i) 100x mag, ii) 200x mag, iii) 1000x mag.

Figure S2.3. Particle size distribution of Gangotri medial moraine samples (see Figure 4).

Figure S2.4. Mean weight percentages per ½ Φ interval of medial moraine samples from Gangotri glacier and comparisons derived from Owen et al. (2003). These comparisons include supraglacial debris from Rakhiot, Chungphur and Glacier de Cheilon (Owen et al. 2003) in addition to Glacier de Tsidijore Nourve (Small 1983), Breidamerkurjokkull, Sore Buchananisen, and the Glacier d'Argentiere (Boulton 1978).

Figure S2.5. Roundness and Sphericity Index for individual grain size fractions of Gangotri medial moraine samples. A) coarse-medium gravel, B) fine gravel, C) coarse-medium sand, D) fine sand, E) silt-clay, F) sample summary (appears as Fig. x).

Figure S2.6. Clast shape of Gangotri medial moraine samples (ternary diagrams using methods of Graham and Midgley, 2000). upper) Clast shape categories defined by Snead and Folk (1958).

Figure S2.7. Percentage surface weathering of quartz sand grains for the Gangotri glacier medial moraines.

Figure S2.8. Diffraction patterns of the clay component of Gangotri medial moraine samples (CT: 1.0 s, SS: 0.05°). A) G_{sup1}. B) G_{sup2}. C) G_{sup3}. D) G_{sup4}. E) G_{sup5}. F) G_{sup6}.

Table S2.1. Percentage grain size distribution of Gangotri medial moraine samples.

Figure S3.1. Slope map with hillshade for the upper Bhagirathi catchment.

Figure S3.2. A) Example ^{10}Be production rate map for the Kirti. B) Accumulation of ^{10}Be during burial, englacial transport and exhumation between rockwall and medial moraine for the Kirti tributary catchment. Additional ^{10}Be inventory is 2500 at/g (u: mean glacier surface velocity [20±5 m/a], X_{ELA}: 3400 m.)

Table S3.1. Analytical model variables to calculate the ^{10}Be inventory gained during transport of rock particles from bedrock slope to medial moraine.

Table S3.2. Potential ^{10}Be accumulation in sediment from medial moraine

Data S1. Supporting information